Atomic-level insights into transition mechanism of dominant mixing modes of multi-component fuel droplets: from evaporation to diffusion

Yifei Gong[a], Kai Hong Luo[b], Xiao Ma[a,*], Shijin Shuai[a], Hongming Xu[a,c]

[a] State Key Laboratory of Automotive Safety and Energy, Tsinghua University, Beijing 100084, China

[b] Department of Mechanical Engineering, University College London, Torrington Place, London WC1E 7JE, UK

[c] Department of Mechanical Engineering, University of Birmingham, Birmingham B15 2TT, UK

Abstract: For a multi-component hydrocarbon mixture under supercritical conditions, especially for fuels injected into compression ignition engines, the mechanism for the transition of the dominant mixing mode from evaporation to diffusion is not well established. In this paper, evaporation processes of a six-component hydrocarbon fuel (13.16 mol% toluene, 13.81 mol% n-decane, 22.30 mol% n-dodecane, 24.60 mol% n-tetradecane, 14.66 mol% n-hexadecane and 11.47 mol% n-octadecane) droplet in nitrogen environments were studied using molecular dynamics (MD) simulations, in comparison with those of three-component and single-component fuel droplets. The ambient pressure ranged from 2 MPa to 16 MPa and the ambient temperature ranged from 750 K to 1350 K. Results indicated that the transition characteristics of the mixed fuel were not the linearly weighted average of the physical properties of individual components in the mixture based on their mole fractions. The reason why there is a limitation on the maximum transition temperature when diffusion dominates the fuel-ambient gas mixing process under high pressures has been discussed. The average resultant force on a fuel atom of an individual component increases with increasing pressure or decreasing temperature at the supercritical temperature, and diffusion will gradually dominate the mixing process of the fuel. The clustering behavior of fuels under supercritical conditions has also been discussed.

Keywords: Multi-component fuels; Droplet evaporation; Supercritical conditions; Mixing transition mechanism; Molecular interactions; Fuel clusters

1. Introduction

Traditional fossil fuels, for example hydrocarbons, have been widely used to power the world economy so far. However, this leads to increasing depletion of fossil energy and a large amount of greenhouse gas emissions. Therefore, improving the utilization efficiency of fossil fuels and reducing emissions have motivated many research efforts. For most power devices such as internal combustion engines (ICEs), this requires combustion of hydrocarbon fuels under high-pressure and high-temperature conditions [1-3]. As a result, the maximum ambient pressure and temperature in combustion chambers of modern engines are getting higher and higher, which tend to exceed the critical points of injected fuels [4-6], especially in compression ignition engines [7, 8]. Once the ambient reaches the critical conditions, the dominant mixing mode of the fuel may transition from evaporation to diffusion [9-12], which strongly influences the subsequent combustion and formation of pollutants [13-17].

Hydrocarbon fuels usually achieve mixing with the ambient gas in the form of droplet evaporation in engines [18-20]. There will be significant changes in the mixing process of droplets if it is dominated by diffusion rather than evaporation [9, 21-25]. Several comprehensive reviews have been focused on the phenomenological differences in the mixing of droplets under sub- and supercritical conditions [26-29]. The traditional droplet evaporation theory, CFD simulations and droplet experiments have been widely used to study the transition behavior of droplets under supercritical conditions in detail [4, 9], although these methods are unable to resolve the nanoscale liquid-gas interfaces. In recent years, molecular dynamics (MD) has been increasingly applied to the study of phase transitions of fuel droplets [4, 30-39]. MD simulations are very suitable for investigating the interfacial behaviors of droplets at atomic scales under both subcritical and supercritical conditions, thus offering a possibility for revealing the mechanisms behind mixing mode transition [30, 40]. Due to the large gap in the droplet size investigated in MD simulations and experiments, the droplet size effects have been investigated in MD simulations [4, 41, 42], although this is a continuing process. It is worth mentioning that MD simulations

of large molecule systems are computationally very expensive and require significant supercomputing resources [43].

MD simulations of the evaporation process of single-component hydrocarbon fuels under supercritical conditions have been performed in recent years [4, 30, 39, 41]. However, the simulated ambient conditions in previous studies [4, 41] are not fully consistent with those in modern engines [4, 9, 39]. Moreover, the molecular interactions in fuel evaporation systems have not been investigated in detail, leaving unanswered questions about the intrinsic mechanisms at the atomic level behind the transition characteristics of fuels. Some studies [40, 44-49] were also focused on the inhomogeneity and clustering of supercritical fluids at the atomic level. However, it is not established whether the fuel cluster forms when the dominant mixing mode changes from evaporation to diffusion under supercritical conditions.

The afore-mentioned studies were focused on single-component fuels but the questions about the behaviors of real fuels which are complex mixtures of hundreds of components have not been answered [9, 50]. The mechanism for transition of multi-component hydrocarbons is not well understood due to the complexities in modeling and analysis [51], hindering the application of this technology [52]. So far, there have been very limited MD simulations of the evaporation process of two-component fuels [42, 43, 53, 54]. Chakraborty et al. [34] investigated phase transitions of two-component fuel liquid films under sub- and supercritical conditions and discussed the changes in surface tension. Zhang et al. [59] studied the evaporation process of a two-component n-alkane fuel film and focused on the non-VLE effects under supercritical conditions. However, physical performances of surrogate fuels with multi-components (>2) are more consistent with those of the actual fuel than single-component surrogates [55].Therefore, the construction of more sophisticated surrogate models is essential to matching the chemical properties of real fuels further [56]. Gong et al. [9] investigated the phase transition processes of three-component hydrocarbon fuel droplets in sub- and supercritical nitrogen environments, in comparison with those of single-component n-hexadecane droplets. Based on the quantitative Voronoi tessellation, a new criterion

[9], which was a combination of two dimensionless critical values of Hc = 0.85 and Wc = 0.35, was proposed to determine the transition of the dominant mixing mode from evaporation to diffusion. However, the molecular interactions between fuel components in multi-component fuels have not been investigated in detail.

As mentioned in [55], it is necessary to adopt a surrogate fuel with multi-components to represent the real mixed fuel to investigate transition behaviors under supercritical conditions. In this paper, the evaporation processes of a six-component fuel droplet under sub- and supercritical conditions were investigated using MD simulations, in contrast to those of a three-component droplet and a single-component droplet reported in previous work [9]. This six-component fuel is composed of toluene (13.16 mol%), n-decane (13.81 mol%), n-dodecane (22.30 mol%), n-tetradecane (24.60 mol%), n-hexadecane (14.66 mol%) and n-octadecane (11.47 mol%). The objective of this paper is to obtain atomic-level insights into the mechanism for transition of multi-component hydrocarbons using MD simulations. The dominant mixing mode regimes on the P-T diagram for three types of fuel droplets were presented. Effects of ambient conditions and fuel component types on the interactions between the fuel molecules and the nitrogen molecules were studied. Atomic-level insights into the mechanism of the dominant mixing mode transition of multi-component hydrocarbon fuels were provided. The cluster phenomenon in the evaporation system was discussed at an atomic level.

2. Research methods

2.1 . Interatomic potentials

The Large-scale Atomic/Molecular Massively Parallel Simulator (LAMMPS) was used to carry out all the MD simulations in this paper [4]. In MD simulations, the determination of intermolecular interaction forces is based on the potential model [53]. The United Atom Model (UAM) has been chosen to simulate the evaporation of complex alkanes here due to its good balance between computational

efficiency and precision [9]. In this model, different pseudo-atoms are used to represent different atom groups [57]. The simplified alkane molecule consists of several associated atoms, as shown in Fig. 1.

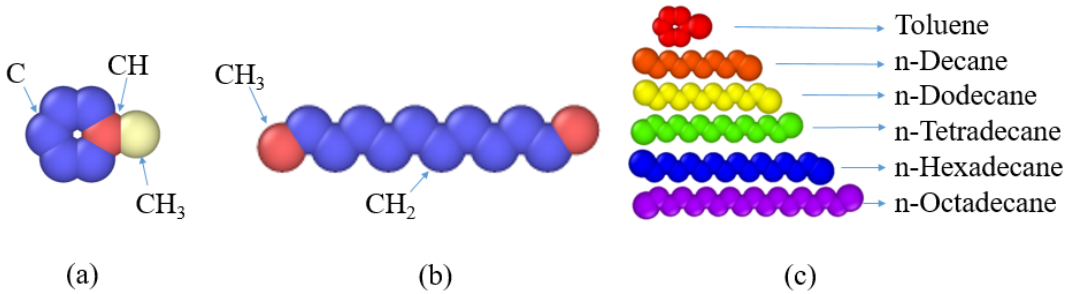

Fig. 1. The schematic diagram of the United Atom Model: (a) Toluene, (b) n-Dodecane and (c) All fuel models used in the six-component fuel droplet.

Following the work of Gong et al. [9], the Transferable Potentials for Phase Equilibria United Atom (TraPPE-UA) Model [58] were used to describe the interactions of fuel molecules. The non-bonded interaction between pseudo-atoms that are separated by more than three bonds or belong to two different molecules is described by the 12-6 Lennard-Jones potential:

$$U^{LJ}(r_{ij}) = 4\varepsilon_{ij}\left[\left(\frac{\sigma_{ij}}{r_{ij}}\right)^{12} - \left(\frac{\sigma_{ij}}{r_{ij}}\right)^{6}\right] \quad (1)$$

where σ_{ij} is the size parameter, ε_{ij} is the energy parameter, and r_{ij} is the distance between the two interacting pseudo-atoms. The LJ parameters for identical pseudo-atoms are listed in Table 1 [58], where k_B is the Boltzmann constant. The LJ parameters for all unlike atoms are determined by the standard Lorentz-Berthelot combining rules [4], $\varepsilon_{ij} = \sqrt{\varepsilon_{ii} \cdot \varepsilon_{jj}}$ and $\sigma_{ij} = (\sigma_{ii} + \sigma_{jj})/2$.

Table 1. Lennard-Jones parameters of the TraPPE-UA force field.

pseudo-atom	ε/k_B [K]	σ [Å]
CH_3(sp3)	98	3.75
CH_2(sp3)	46	3.95
CH(sp2)	47	3.73
C(sp2)	20	3.85

The bond-stretching, bond bending and bond torsion parameters for alkanes have been shown in detail in authors' previous work [9] and are not listed here again. Aromatic molecules are treated as rigid bodies [58]. Each nitrogen molecule is regarded as two atoms connected by a fixed bond length according to the SHAKE algorithm [59]. The model parameters used for nitrogen molecules have been listed in [9].

2.2. Model verification

In this paper, the evaporation processes of a six-component fuel droplet under sub- and supercritical conditions were investigated using MD simulations, in comparison with those of a three-component droplet and a single-component droplet reported in previous work [9]. With reference to the six-component alternative fuel model proposed by Youngchul et al. [60] (toluene (15 mol%), n-decane (14 mol%), n-dodecane (22 mol%), n-tetradecane (24 mol%), n-hexadecane (14 mol%) and n-octadecane (11 mol%)), an initial fuel droplet was used to simulate the thermal equilibrium state at 363 K of it at first. After the equilibrium, a new six-component fuel droplet model was obtained. This six-component fuel is composed of toluene (13.16 mol%), n-decane (13.81 mol%), n-dodecane (22.30 mol%), n-tetradecane (24.60 mol%), n-hexadecane (14.66 mol%) and n-octadecane (11.47 mol%). This alternative fuel is almost the same as the six-component alternative fuel proposed by Youngchul et al. [60]. According to the research of Youngchul et al. [60], their proposed six-component alternative fuel has a very similar distillation curve with the reference diesel Fuel A [61]. The distillation curves of the six-component alternative fuel proposed by Youngchul et al. [60] and Fuel A [61] are shown in Figure 2. The distillation curve of the six-component alternative fuel used in MD simulations is also shown. As seen from Figure 2, the simulation results from CFD [60] have a larger error than the MD results, compared with the experimental values [61], at the beginning of distillation. In the intermediate stage of distillation, the simulation results of CFD and MD are both in good agreement with the experimental values. Near the end of the distillation process, the results obtained by MD simulations have larger errors than those of the CFD

simulations. This is because when the distillation is coming to its end, the droplet size in the MD simulation is already very small, and the error becomes larger. However, even the largest error in MD simulations is acceptable (about 7% at 570 K). In summary, the distillation curve of the six-component alternative fuel used in this paper agrees well with that of the reference diesel Fuel A. This verifies the accuracy of the six-component surrogate fuel model for real diesel and LJ force field parameters used in this paper, both of which can be used for the following simulation of multi-component fuel droplets.

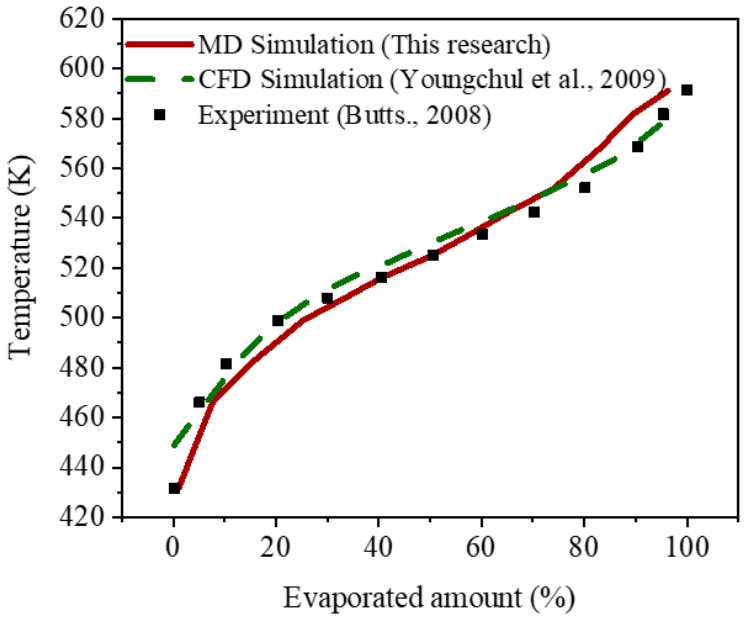

Fig. 2. Comparison of distillation curves of the diesel obtained by three different methods. Redrawn CFD data are based on [60]. The experimental data are from [61].

2.3. Properties of fuels

The critical point of the fuel plays an important role in the transition characteristics under supercritical conditions. In this paper, a theoretical method [62, 63] was adopted to estimate the critical point of the six-component alternative fuel. The estimation equation of the critical temperature of a simple mixture was given by Li et al. [62], and the estimation equation of critical pressure of a mixture was proposed by Kreglewski et al. [63], which are shown in detail in the authors' previous work [9]. The

estimated critical properties (including critical temperature T_c and critical pressure P_c) of the six-component alternative fuel, as well as those of its individual components, are shown in Table 2.

Table 2. Critical points of the fuel.

	T_c [K]	P_c [MPa]
toluene	593	4.1
n-decane	618	2.11
n-dodecane	658	1.81
n-tetradecane	693	1.6
n-hexadecane	722	1.4
n-octadecane	747	1.3
six-component fuel	686	2.45

2.4. Simulation configurations

The initial configuration of the droplet evaporation system is shown in Fig. 3. A single suspended fuel droplet is located in the center of a cubic box and surrounded by a nitrogen ambient. Before the simulations of evaporation of droplets in nitrogen, the fuel droplet and the nitrogen ambient were simulated separately using the canonical ensemble (NVT, which means constant atom number N, constant volume V, and constant temperature T) [41]. When both the fuel and the ambient gas respectively reached their own thermodynamic equilibrium state, the two were combined together. It is worth noting that the nitrogen molecules in the center region of the simulation box were deleted to avoid the overlap of molecules [4]. The initial temperature of the fuel was set to 363 K, close to that of the fuel in real engines before injection.

The size of the simulation box was $120\ \text{nm} \times 120\ \text{nm} \times 120\ \text{nm}$, and periodic boundary conditions were used in all three dimensions. The simulations were performed using the micro-canonical ensemble (NVE, which means constant atom number N, constant volume V, and constant energy E) [30]. The region outside of the sphere with a radius of 40 nm was named “thermostat region”, in which velocities of the

molecules were rescaled every time step using a speed reset method [30]. The translational velocities of the molecules located in this region were rescaled every time step according to

$$V_i^{new} = V_i^{old}\left(\frac{3TN_t k_B}{2E_k}\right)^{0.5} \quad (2)$$

where E_k indicates the total kinetic energy of the N_t atoms in the thermostat region, and T indicates the target ambient temperature. The calculations of temperature in MD simulations are based on the average kinetic energy of molecules [53]:

$$\frac{3}{2}k_B TN = \sum_{i=1}^{N}\frac{1}{2}m_i v_i^2 \quad (3)$$

where N is the number of atoms in the target atom group, m_i and v_i are respectively the mass and velocity of i-th atom. As a consequence, the temperature of this region could be kept at a constant target value. The initial ambient pressure was determined by a combination of the initial ambient temperature and the initial number of nitrogen molecules in the simulation box in NVT simulations. However, the ambient pressure was determined by choosing a suitable initial number of nitrogen molecules in the system in NVE simulations [30]. The number ranges of nitrogen molecules are shown in Table 3. A fuel molecule will be removed when it gets to the thermostat region to simulate the evaporation of the droplet taking place in an infinite space [4]. It is worth mentioning that the droplet accounts for far less than 1% of the volume of the simulation box, so the fluctuations of ambient pressure could be negligible.

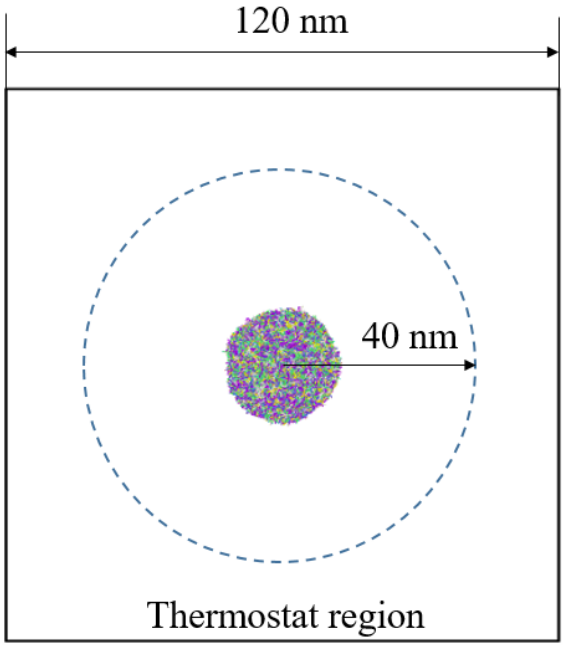

Fig. 3. Initial configurations of the six-component fuel droplet. Blue particles indicate toluene molecules, yellow particles n-decane molecules, purple particles n-dodecane molecules, green particles n-tetradecane molecules, dark blue particles n-hexadecane molecules and grey particles n-octadecane molecules. Nitrogen molecules surround the droplet, which are not shown here.

Initially, the six-component droplet contained 18,150 fuel molecules, forming an initial diameter of 24.3 nm. Other details are summarized in Table 3. Considering both potential subcritical and supercritical conditions occurred in real diesel engines [30, 53], the target ambient temperature and the target ambient pressure of simulations for the six-component fuel droplets were in the range of 750-1350 K and 2-16 MPa, respectively. Taking into account the operating conditions before fuel injection [30], the maximum ambient temperature (1350 K) and the maximum ambient pressure (16 MPa) were chosen in this research. The minimum ambient temperature (750 K) and the minimum ambient pressure (2 MPa) were selected here to simulate the traditional droplet evaporation behavior. Compared with the authors' previous work [9], the investigated ambient conditions of the three-component and the single-component fuel droplets were applied to that of the six-component fuel droplets for further investigating multi-component effects in transition behaviors of fuels. The reduced ambient temperature T_r and the reduced

ambient pressure P_r are both calculated by dividing ambient values by critical values of the fuel. The integral of the equation of motion was carried out by the velocity-Verlet algorithm [64]. The time step is 2.0 femtosecond in all cases. The total time steps for a certain case differed with the droplet evaporation lifetime.

Table 3. Simulation details of six-component fuel droplets.

Physical parameters	Value
Initial number of fuel molecules in the droplet	2389 (toluene, 13.16 mol%) 2507 (n-decane, 13.81 mol%) 4047 (n-dodecane, 22.30 mol%) 4464 (n-tetradecane, 24.60 mol%) 2661 (n-hexadecane, 14.66 mol%) 2082 (n-octadecane, 11.47 mol%)
Initial droplet diameter, nm	24.3
Initial droplet temperature, K	363
Initial number of nitrogen molecules	206436 - 2606935
Ambient pressure, MPa	2-16
Ambient temperature, K	750-1350

A similar initial configuration for multi-component droplet MD model has been carefully verified in previous work [9].

3. Results and discussion

3.1. Dominant mixing mode maps for several hydrocarbon fuels

Based on the criteria of the quantitative Voronoi tessellation proposed in the authors' previous work [9], the dominant mixed mode maps of 6-component droplets, 3-component droplets and single-component droplets were obtained in this study, as shown in Fig. 4a and b. The maps of the three-

component droplet and the single-component droplet were extended on the basis of the original work [9] (this paper extended the ambient pressure to more than 10 MPa and extended the ambient temperature to 1350 K, respectively) to compare with that of 6-component droplets. In addition, the transition processes of n-hexadecane and n-dodecane in several fuels have also been investigated emphatically and compared, as shown in Figs. 4c and d.

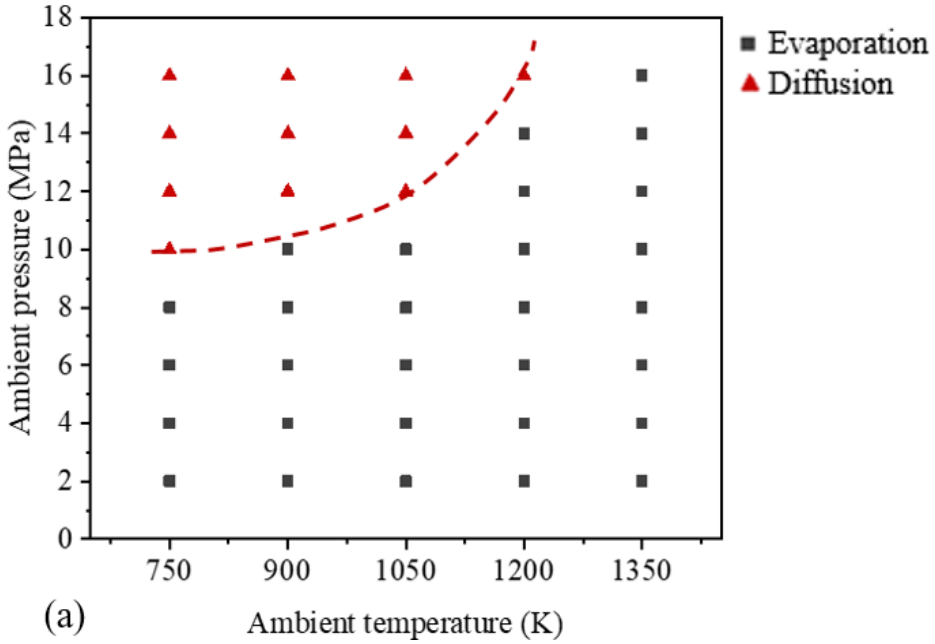

(a)

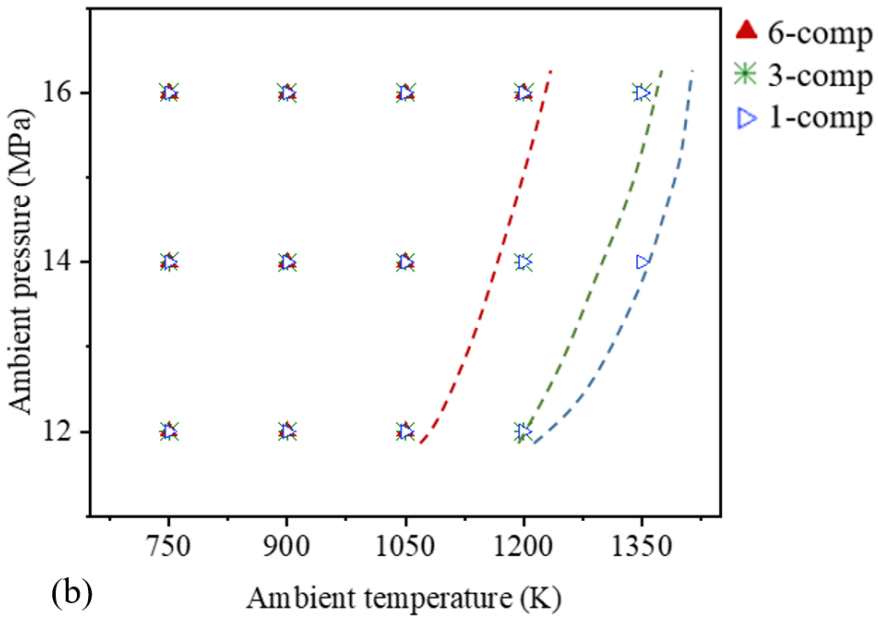

(b)

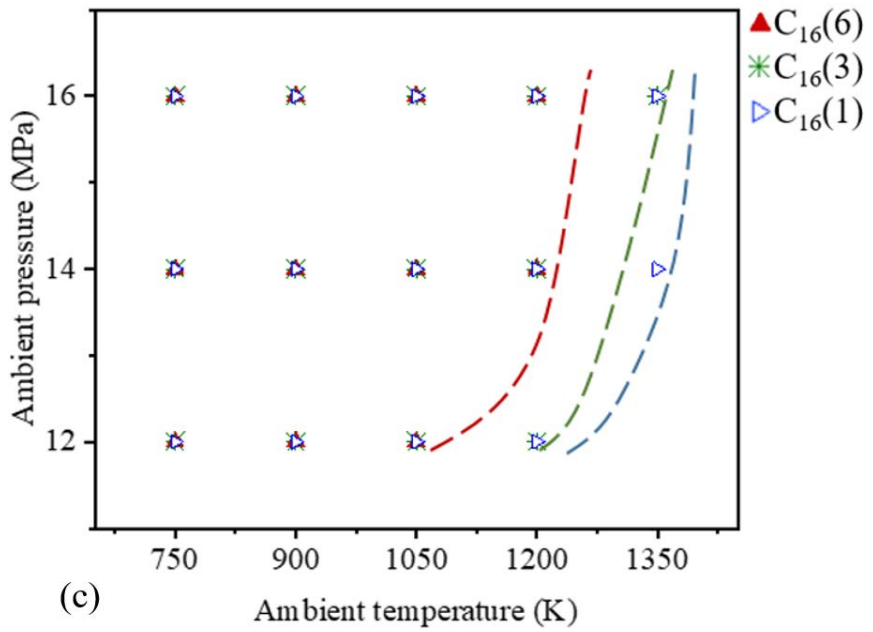

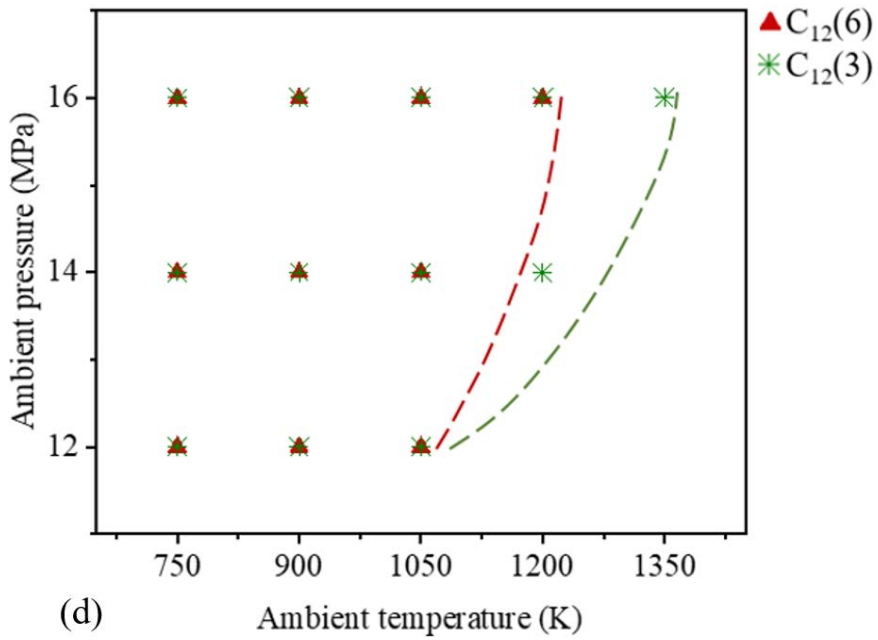

Fig. 4. The dominant mixing mode maps: (a) Six-component fuel droplets, (b) Six-component fuel droplets, three-component fuel droplets and single-component fuel droplets, (c) n-Hexadecane in three fuel droplets and (d) n-Dodecane in two fuel droplets.

As shown in Figure 4a, within the ambient conditions studied in this paper, the minimum pressure at which the transition of dominant mixing modes for the 6-component droplet occurs is 10 MPa. Below this pressure, no transition occurs in the temperature range investigated here. The maximum temperature at

which the fuel can transition (namely the maximum transition temperature at certain pressure) increases with increasing ambient pressure, which is consistent with the previous conclusions of single-component droplets [9]. More details on the mechanism for transition of dominant mixing modes of the single-component fuel have been discussed in the authors' previous work [9]. It is worth mentioning that the transition profiles are not similar to those proposed by Poursadegh et al. [7, 8]. In their research [7, 8], following Dahms et al. [5, 13, 65], equation of state and linear gradient theory [66] were applied to investigate the spray regime diagram. The dominant mixing mode maps obtained here are based on the quantitative Voronoi tessellation analysis [9]. This method is suitable for resolving the local distribution of molecule systems at an atomic level and widely used for supercritical fluids [40, 45], which is very different from the theoretical model adopted by Poursadegh et al. [7, 8] that focuses on the macroscopic physics and analysis of thermodynamic states of fluids. What needs to be emphasized is that the transition criteria in the fuel-ambient gas mixing system under supercritical conditions have not been unified, which motivates many research efforts [9, 13, 53, 67]. As reported [7, 8, 13, 68], the surface tension, an unbalanced internal molecular interaction, a crucial parameter in the definition of spray regimes, decreases with increasing ambient pressure or temperature. This finding is consistent with the profiles of internal molecular interactions obtained in this research, which will be discussed in Section 3.3.1. Figure 4b shows the comparison of maps for 6-component, 3-component and single-component droplets when the pressure exceeds 12 MPa. As can be seen from Fig. 4b, at the same pressure, the maximum transition temperature of the 6-component droplet is the smallest among those of the three fuels. In other words, under the same temperature, the minimum pressure at which 6-component droplets can transition (namely minimum transition pressure at certain temperature) is the highest among the three fuels. At the same temperature, the minimum transition pressure of the 3-component droplet is slightly higher than that of the single-component droplet, which is consistent with previous research conclusions [9]. As for the relative molecular mass, for the 6-component, 3-component and single-component fuel studied in this paper, it is

180.95, 206.03 and 226.44, respectively. As shown in Table 3, for an individual fuel component, the lower the relative molecular mass is, the higher the critical pressure will be and the lower the critical temperature will be. For a mixed fuel, when the relative molecular mass of it gets lower, the minimum transition pressure at certain temperature will increase and the maximum transition temperature at certain pressure will decrease, as shown in Fig. 4b.

However, this study has proved that the transition characteristics of the mixed fuel are strongly related to the interactive forces between the atoms in the fuel. And the intermolecular force of the mixed fuel is not the weighted average of that of the individual fuel components. Therefore, the transition characteristics of the mixed fuel would not be the linearly weighted averages of the physical properties of individual components in the mixture based on their mole fractions. These will be analyzed in detail below. This provides intrinsic mechanisms at the atomic level for the published experimental research [69] in which only phenomenological results could be obtained. Figure 4c shows the dominant mixing mode map of n-hexadecane in the three fuels. It can be seen that for the same component, because different fuels have different intermolecular forces, even under the same ambient conditions, the dominant mixing modes of n-hexadecane in different fuels are different. Similar to Figure 4b, at the same ambient temperature, the minimum transition pressure of n-hexadecane in the 6-component droplet is the highest, followed by that of n-hexadecane in the 3-component droplet. The minimum transition pressure of n-hexadecane droplets is close to that of 3-component droplets, but overall it is the smallest among the three fuels. Figure 4d shows the dominant mixing mode map of n-dodecane in the three fuels. The situation of n-dodecane is similar to that of n-hexadecane. At the same ambient temperature, the minimum transition pressure of n-dodecane in the 6-component droplet is higher than that of the n-dodecane in the 3-component droplet. This indicates that the transition of a certain component in the mixed fuel will be affected by other components. The following conclusion can be drawn from Figs. 4c and d. For a certain pure component

in the mixed fuel, the minimum transition pressure of it at certain temperature will increase with the decreasing relative molecular mass of the mixed fuel.

3.2 Mixing characteristics of multi-component droplets in different dominant mixing modes

The definitions of droplets are from [4]. The boundary of the droplet is defined as the contour surface where the density is equal to the average of the maximum density and the minimum density of the evaporation system. The diameter of the droplet is defined as that of a sphere of the same volume as the droplet. Figure 5 shows profiles of the dimensionless square diameter $(d/d_0)^2$ of the droplet with time normalized by d_0^2. The method of least squares linear fitting is used to fit the data points located in the range of 0.862 d_0^2 to 0.215 d_0^2 (corresponding to the initial droplet volume of 80% to 10%), and the slope of the fitting straight line is defined as the evaporation rate constant *k*. The time corresponding to the intersection point of the fitting line and the straight linear $d^2 = d_0^2$ or the straight linear $d^2 = 0$ is defined as the initial heat-up time t_h and the droplet evaporation lifetime t_L , respectively, as shown in Fig. 5. In the evaporation process, the droplet has a volume expansion at the initial stage due to the thermal expansion and the adsorption and dissolution of nitrogen molecules on the droplet [9], causing a slow evaporation and a minus evaporation rate. After the droplet volume reaching its maximum, the evaporation experiences a short transition period and the evaporation rate gradually increases with time. After that, the droplet evaporates following the classic "D^2" law [4], during which the evaporate rate calculated based on the square diameter remains constant until the droplet vanishes.

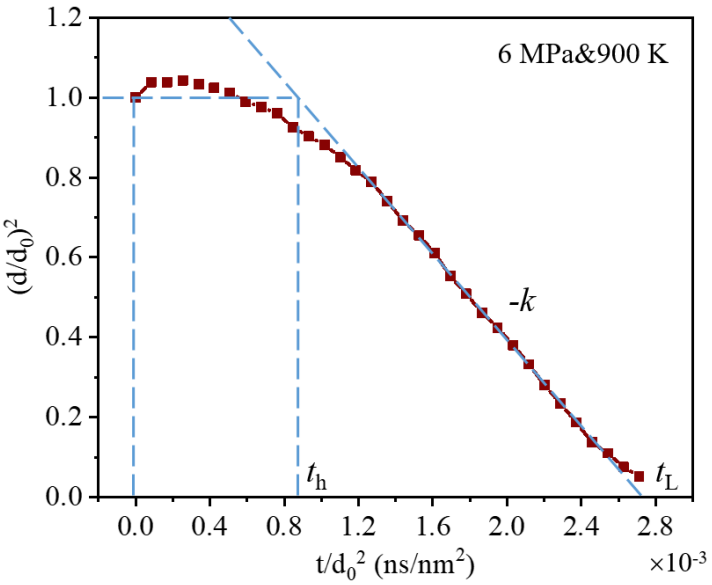

293

294 **Fig. 5.** The temporal variation of the dimensionless square diameter $(d/d_0)^2$ of the six-component droplet.

295 Figure 6 shows the evaporation histories of the molecular number and molar fraction of droplets of
296 six-component droplets in different dominant mixing modes. According to the classification of Fig. 4a,
297 Figure 6a shows the situation of evaporation-dominated mixing. As seen from Figure 6a, the evaporation
298 rates of different fuel components are different. In the first 0.4 ns of evaporation, the number of toluene
299 molecules in the droplet is reduced by about 900, while that of n-octadecane molecules is only reduced
300 by about 400. In addition, during the evaporation of the droplet, a lot of nitrogen molecules dissolve into
301 the fuel droplets, and the number of them reaches a peak of about 1600 at about 0.45 ns. As shown in
302 Figure 6b, before the end of evaporation, the molar fraction of light components such as toluene and n-
303 decane in the droplets gradually decreases with time, the mole fraction of n-tetradecane remains basically
304 unchanged, while the molar fraction of heavy components such as octadecane gradually increases. The
305 molar fraction of the nitrogen molecules in the droplets gradually rises with time, and has a sharp increase
306 near the end of the evaporation. Figure 6c shows the situation of diffusion-dominated mixing. When the
307 pressure increases from 6 MPa to 16 MPa, the difference in evaporation rate of different fuel components
308 is greatly reduced during the mixing process. In the first 0.4 ns of mixing, the number of toluene molecules
309 in the droplet decreases by about 1000, and the number of n-octadecane molecules decreases by 700. In

addition, due to the rapid disappearance of the droplet interface, nitrogen molecules dramatically dissolve into the fuel droplets, and their number reaches a peak of about 4000 at 0.4 ns. As shown in Figure 6d, before the end of mixing, the molar fraction of all fuel components in the droplets gradually decreases with time, while the mole fraction of nitrogen molecules in the droplets rises rapidly with time. At the end of the evaporation, the molar fraction of nitrogen molecules has exceeded 50%. The evaporation rate of individual components increases with increasing temperature from 900 K to 1200 K at a pressure of 16 MPa, as shown in Figure 6e. Within the first 0.4 ns of mixing, the number of toluene molecules in the droplet decreases by about 1500, and that of n-octadecane molecules decreases by 1100. Moreover, the number of nitrogen molecules in the droplet reaches a peak of about 2400 around 0.2 ns, which drops to 60% of the peak number of nitrogen molecules under low temperature conditions (16 MPa and 900 K). This is the reason why there is a limitation on the maximum transition temperature when diffusion dominates the fuel-ambient gas mixing process. When the pressure is not lower than the minimum transition pressure and the temperature is at critical one, once the increasing temperature exceeds the maximum transition temperature at this pressure, the dominant mixing mode will change from diffusion to evaporation. The diffusion-dominated mixing process is accompanied by a massive dissolution of nitrogen in the droplets. When the “nitrogen + hydrocarbon fuel” binary system is at a supercritical temperature (relative to the fuel), the dominant mixing mode transition will occur if the ambient pressure is not lower than the minimum transition pressure and the ambient temperature is not higher than the maximum transition temperature.

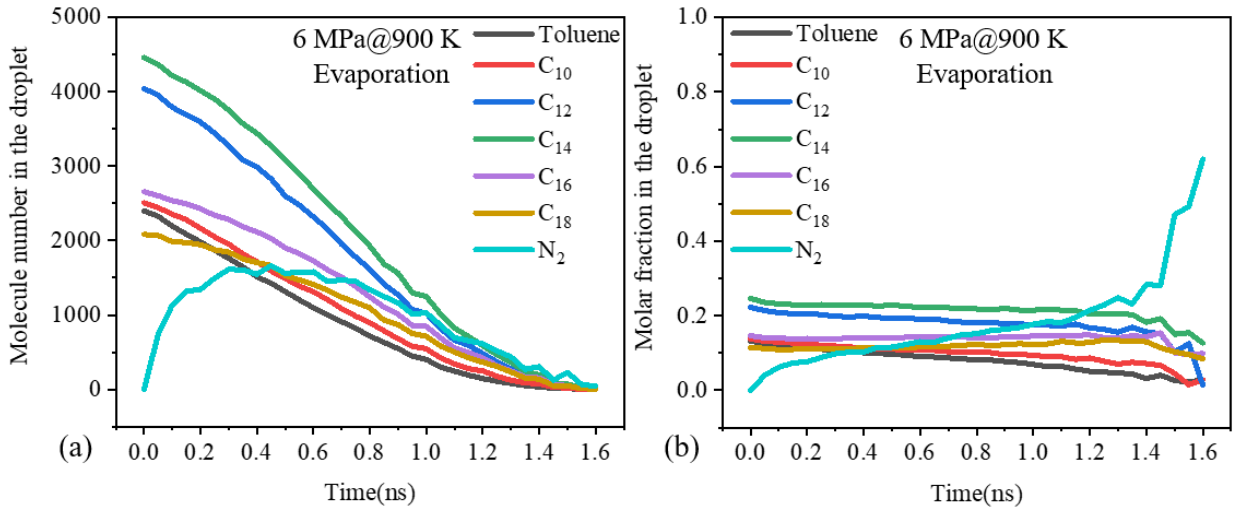
6 MPa@900 K
Evaporation
Toluene
C10
C12
C14
C16
C18
N2
Molecule number in the droplet
Molar fraction in the droplet
Time(ns)
(a)
(b)

329

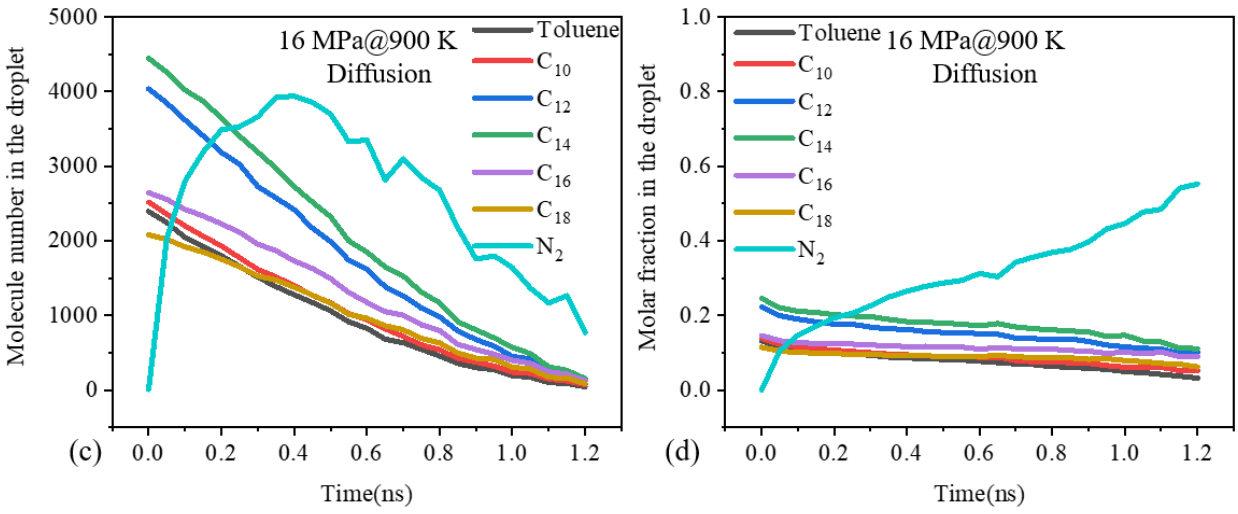
16 MPa@900 K
Diffusion
Toluene
C10
C12
C14
C16
C18
N2
Molecule number in the droplet
Molar fraction in the droplet
Time(ns)
(c)
(d)

330

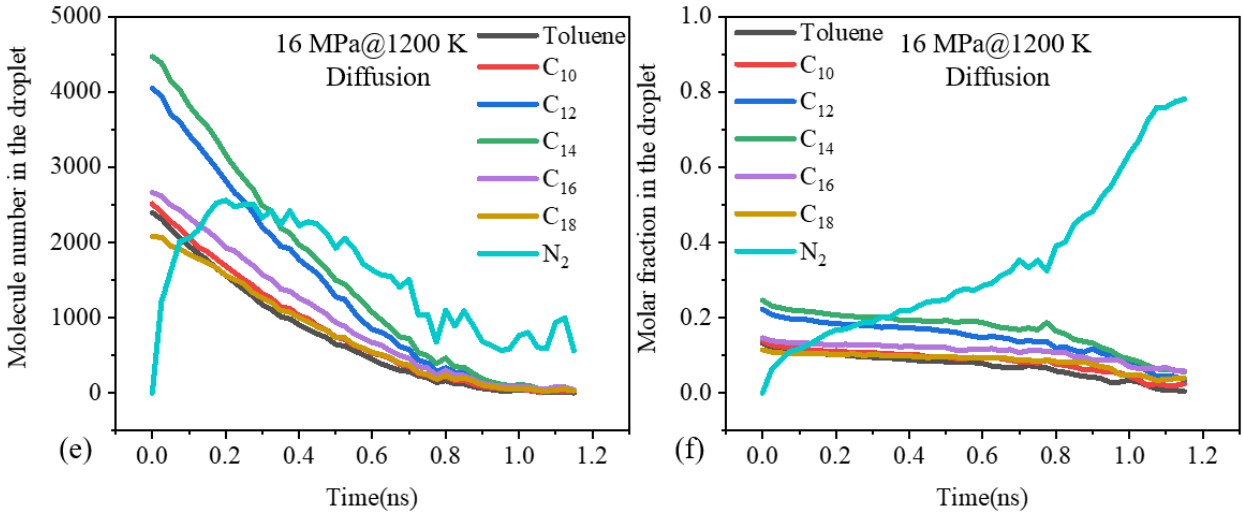
16 MPa@1200 K
Diffusion
Toluene
C10
C12
C14
C16
C18
N2
Molecule number in the droplet
Molar fraction in the droplet
Time(ns)
(e)
(f)

331

Fig. 6. Comparisons of evaporation histories of six-component droplets in different dominant mixing modes: (a) Molecule number (6 MPa and 900 K), (b) Molar fraction (6 MPa and 900 K), (c) Molecule number (16 MPa and 900 K), (d) Molar fraction (16 MPa and 900 K), (e) Molecule number (16 MPa and 1200 K) and (f) Molar fraction (16 MPa and 1200 K).

Figure 7 shows the density distribution of fuel and nitrogen in the six-component droplet system under different dominant mixing modes. As shown in Figure 7a, when evaporation dominates the mixing (6 MPa and 900 K), the average density of the fuel decreases from 3.75 mol/L to 1.75 mol/L at initial 1 ns of evaporation. Meanwhile, a large density gradient is always maintained near the droplet vapor-liquid interface. However, when diffusion dominates the mixing (16 MPa and 900 K), the average density of the fuel dramatically falls from 3.75 mol/L to less than 1 mol/L due to the dramatic dissolution of nitrogen in the droplets at initial 1 ns of mixing, as shown in Figure 7b. The density gradient of the fuel near the droplet vapor-liquid interface decreases, and the density curve becomes smoother. It is worth noting that no matter what dominant mixing modes, at the initial stage of evaporation (t = 0.2 ns), nitrogen molecules are enriched on the surface of the droplets. A similar phenomenon occurring in other systems has also been observed recently [54, 70]. This is because the attraction of the droplet to the nitrogen molecules near the adjacent interface is much greater than that of the nitrogen molecules to themselves, so the nitrogen molecules are attracted to the surface of the droplet. As the fuel-ambient gas mixing progresses, this enrichment phenomenon gradually disappears. It can be seen from the nitrogen density curves in Figs. 7a-b that the enrichment phenomenon is more obvious at low pressures. Under the ambient condition of 6 MPa and 900 K, the proportion of nitrogen peak density exceeding the bulk density of nitrogen is 21.4% ($\frac{1.117-0.92}{0.92} = 0.214$) at t = 0.2 ns. However, under the ambient condition of 16 MPa and 900 K, that one falls to 13.3% ($\frac{2.657-2.345}{2.345} = 0.133$) at t = 0.2 ns. This is because as the number density of nitrogen molecules increases at high pressure, the attraction of bulk nitrogen to nitrogen molecules adjacent to the droplet interface increases. As a result, fewer nitrogen molecules are adsorbed on the droplet surface. As

previously reported [9], the accumulation of nitrogen molecules on the droplet surface at the initial stage of evaporation is also an important reason for the initial volume expansion of the droplet.

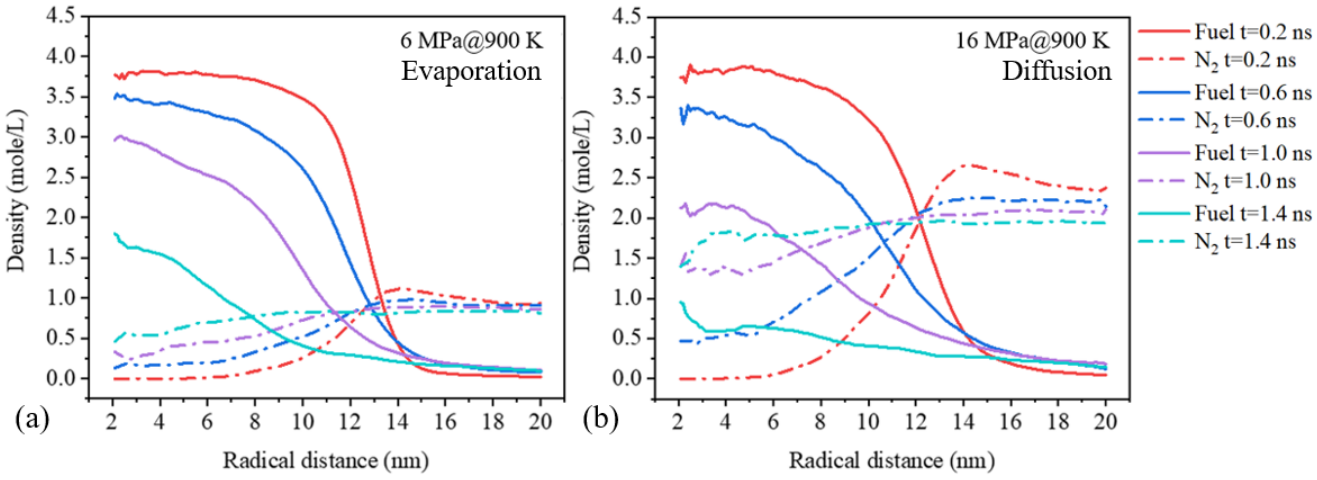

Fig. 7. Density profiles of six-component droplets in different dominant mixing modes: (a) Evaporation and (b) Diffusion.

Figure 8 shows the temperature history of droplets in different dominant mixing modes. The initial temperature of the liquid fuel is 363 K. At the initial stage of droplet evaporation, the temperature near the droplet interface differs greatly from that in the far-field. The droplet absorbs heat from the ambient during the evaporation process, and the temperature near the interface decreases. With heat transfer, the temperature difference between the fuel and the ambient gas decreases, and the temperature varies more smoothly along the radial direction of the droplet. In the evaporation mode (6 MPa@900 K), the droplet boundary is sharp, and the temperature profile falls sharply near the droplet interface (the instantaneous droplet radii have been indicated in Figure 8). In the diffusion mode (16 MPa@900 K), however, the phase boundary of the droplet gradually disappears with time. Consequently, compared with the case of evaporation, the temperature profile varies more smoothly along the radial direction at the same time and has not an apparent turning point.

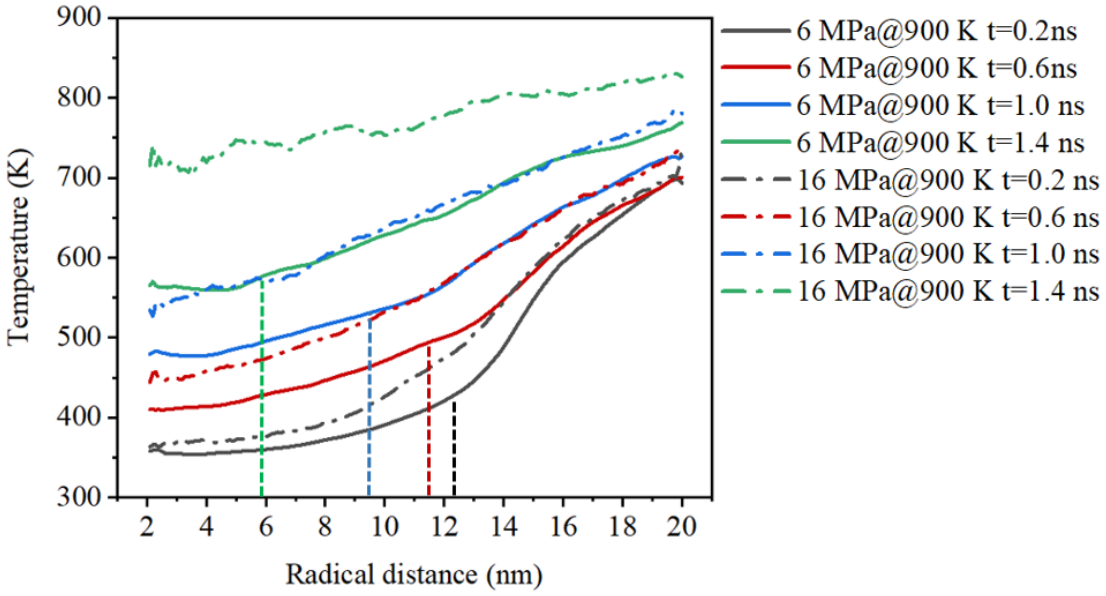

372

373 **Fig. 8.** Temperature histories of six-component droplets in different dominant mixing modes. The dotted
374 line indicates the radius of the fuel droplet at a certain moment.

375 Figure 9 shows temporal variations of the average energy per fuel atom of the six-component droplet
376 in evaporation mode (6 MPa and 900 K). Figure 10 shows the temporal variations of ratio (C_{18}/C_{10}) of
377 average energy per fuel atom of a typical heavy component n-octadecane to a typical light component n-
378 decane when six-component droplets are in different dominant mixing modes. When evaporation
379 dominates the mixing process, the lower the relative molecular mass of a fuel component, the greater the
380 average kinetic energy of each atom at the same time, as shown in Figures 9 and 10. As for the potential
381 energy, at the beginning of evaporation, because the relative molecular mass of the long-chain molecule
382 is larger and the structure of it is more complex, the potential energy inside the molecule is larger. As a
383 result, the average potential energy per fuel atom is larger, as shown in Figure 9. Since evaporation
384 dominates the fuel-ambient gas mixing process, the short-chain light components evaporate first, causing
385 the distance between molecules increasing. Although the light components that evaporate first have more
386 nitrogen molecules around than heavy components at a certain moment, the pressure at this time is lower
387 (6 MPa). Under this circumstance, the number density of nitrogen molecules is lower, and the potential

energy per fuel atom of the light component is dominated by the pair potential between fuel molecules. Therefore, the average potential energy per atom of short-chain light components increases, temporarily surpassing that of the long-chain heavy molecules. However, the average potential energy per atom of them gets lower than that of heavy molecules once again at t = 1.0 ns, as can be seen from Figure 10. Under the condition of 16 MPa and 900 K, diffusion dominates the fuel-ambient gas mixing process and the difference of kinetic energy among fuel components decreases at a certain moment, as shown in Figure 10. Meanwhile, the average potential energy per atom of n-octadecane is greater than that of n-decane at almost the whole mixing time, proving that the light and heavy components start mixing almost at the same time, different from the sequential evaporation in the evaporation mode.

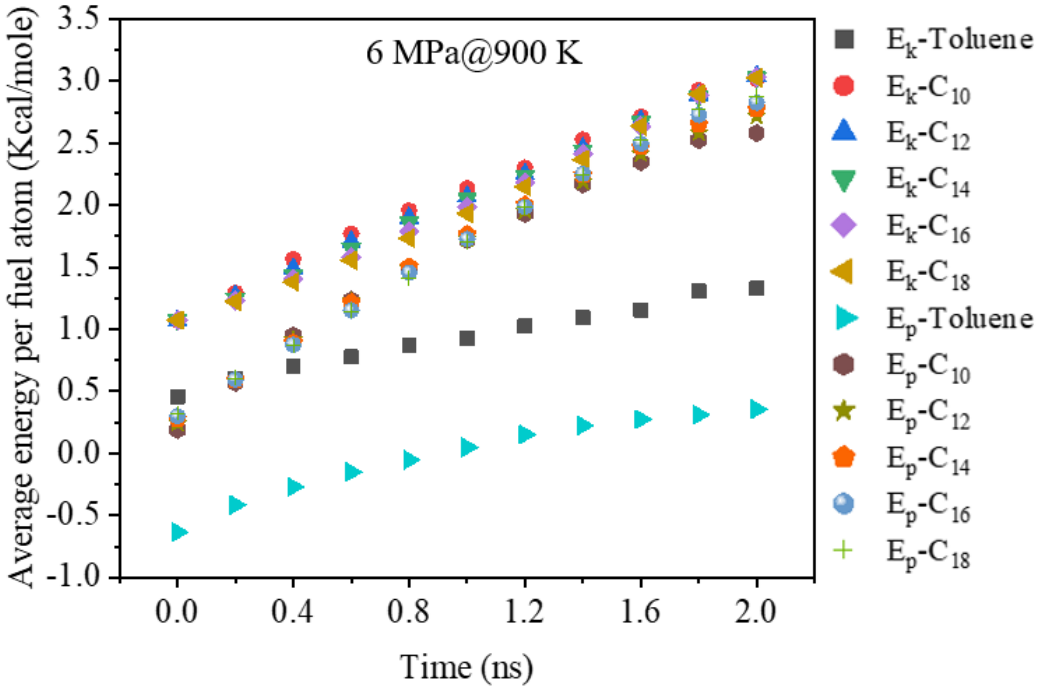

Fig. 9. Temporal variations of average energy per fuel atom of the six-component droplet.

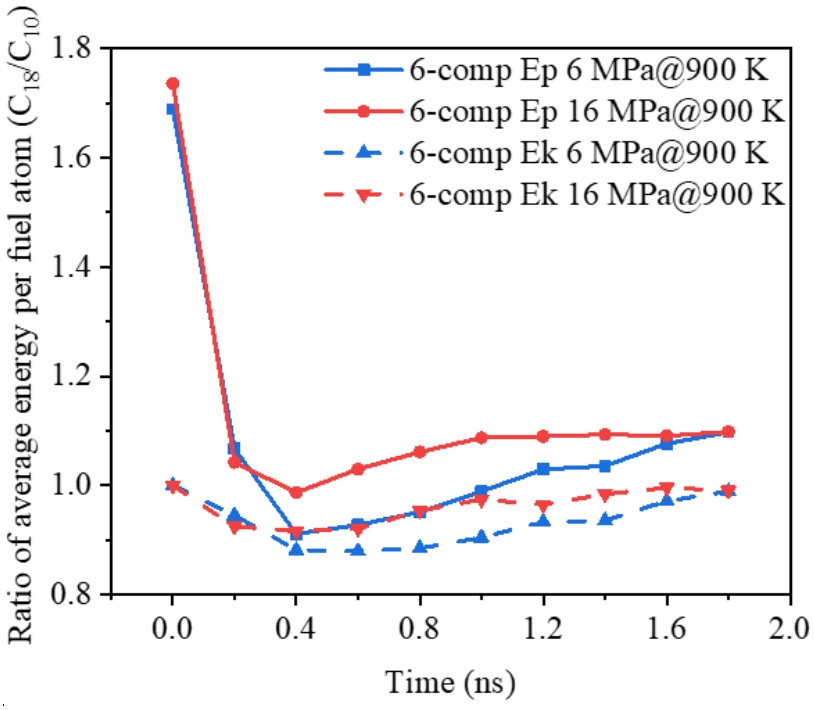

Fig. 10. Temporal variations of ratio of average energy per fuel atom (C_{18}/C_{10}) of the six-component droplet.

3.3 Transition mechanism for the dominant mixing mode of multi-component fuel droplets

3.3.1 Atomic-level insights into the interactive force and energy transfer of the fuel droplet system

The symbol F_{pfa} denotes the average resultant force on each atom of an individual component in mixed fuel droplets by all the other atoms in the system in this paper. Figures 11-12 respectively show the profiles of F_{pfa} in the 6-component droplet system and the 3-component droplet system. It can be seen from Figure 11a-b that in the 6-component droplets studied in this paper, under the same environmental conditions, F_{pfa} decreases first and then increases with the increasing number of C atoms contained in fuel molecules. As shown in Figure 11a, when the temperature increases at an ambient pressure of 6 MPa, F_{pfa} decreases at the same time (for the light components toluene and n-decane, F_{pfa} of them increases slightly in the later period of evaporation process). However, when the pressure increases at an ambient temperature of 1200 K, F_{pfa} increases at the same time. As shown in Figure 12a-b, in the three-component

droplets studied in this paper, under the same environmental conditions, F_{pfa} gradually decreases with the increasing number of C atoms contained in fuel molecules. As shown in Figure 12a, when the temperature increases under an ambient pressure of 6 MPa, F_{pfa} decreases at the same time on the whole (for the light component isooctane, F_{pfa} increases slightly at the end of its evaporation process). Similarly, as shown in Figure 12b, when the pressure increases at an ambient temperature of 1200 K, F_{pfa} increases at the same time on the whole. In addition, as shown in Figures 11 and 12, for a certain pure component, F_{pfa} is different in different mixed systems, resulting in its different transition points. In other words, the composition of the mixed system has an important influence on the transition behaviors of each pure component, as shown in Figure 4c-d. For the same mixed fuel evaporation system (the same mixed fuel and the same ambient gas) at the supercritical temperature, F_{pfa} increases with increasing pressure at constant temperature. As a result, diffusion will gradually dominate the mixing process of the component. However, F_{pfa} decreases with increasing temperature at constant pressure. Consequently, evaporation will gradually dominate the mixing process of the component. These findings provide atomic-level insights into the phenomena reported previously [9].

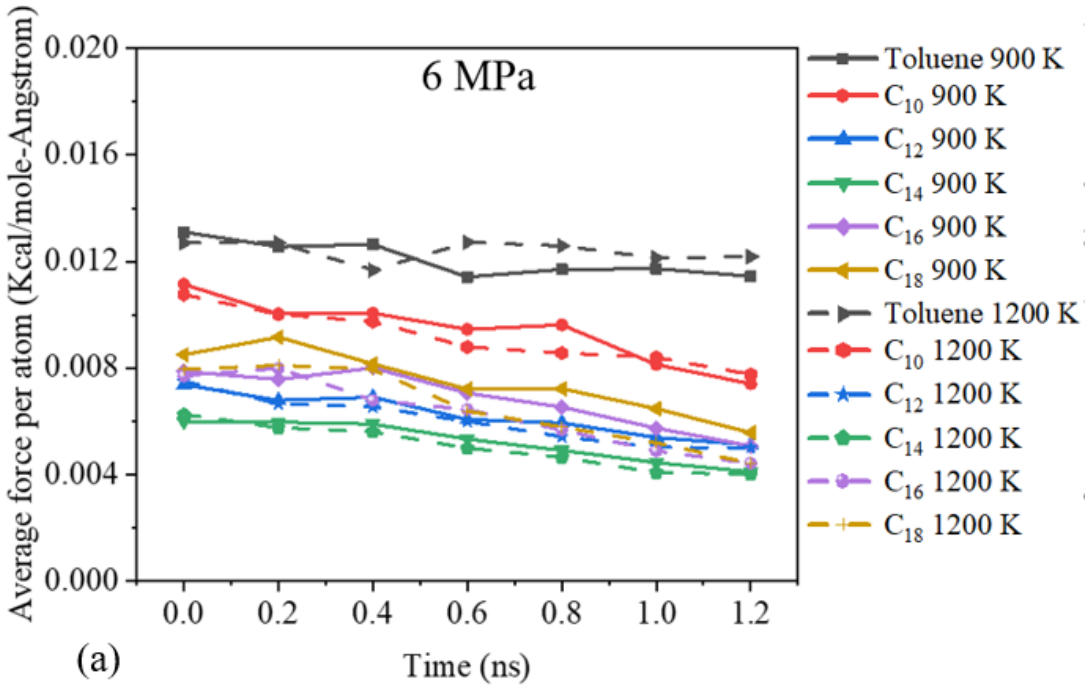

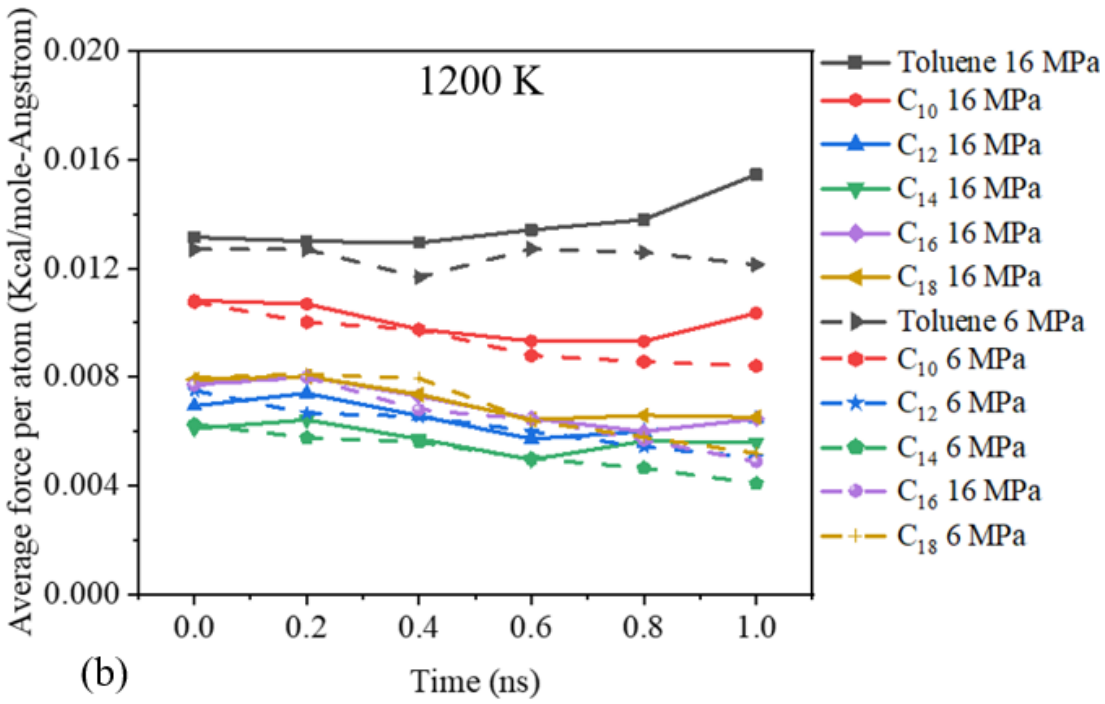

428

429 **Fig. 11.** Average resultant force on each atom of every component in six-component fuel droplets by all

430 the other atoms in the system: (a) 6 MPa and (b) 1200 K.

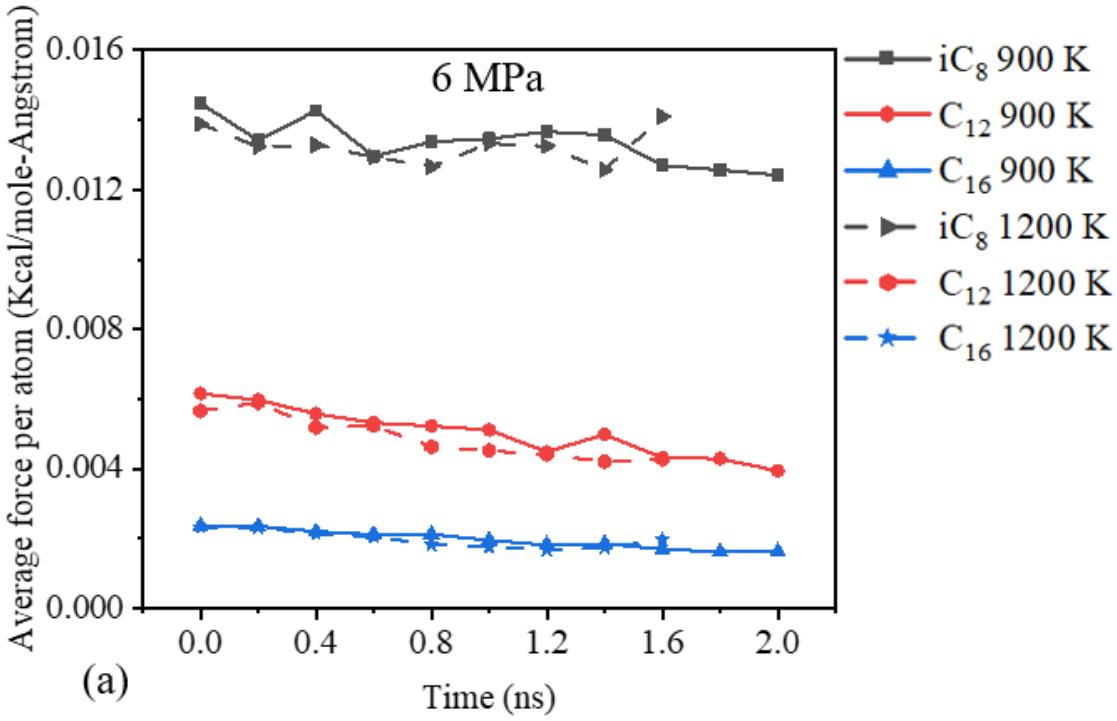

431

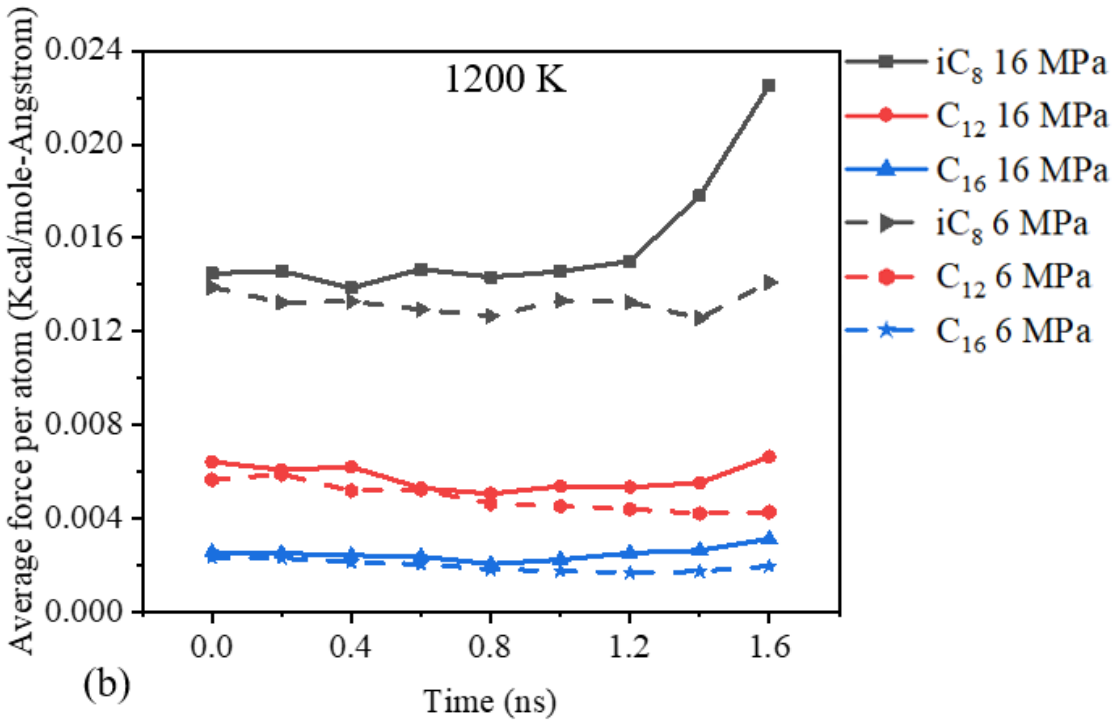

Fig. 12. Average resultant force on each atom of every component in three-component fuel droplets by all the other atoms in the system: (a) 6 MPa and (b) 1200 K.

The profiles of F_{pfa} has been discussed above. The physical mechanisms behind will be explained further. There is no doubt that the external force on a certain fuel component derives from the ambient nitrogen molecules and all the other fuel components in the droplet. The symbol F_{npfa} denotes the average resultant force on each fuel atom by nitrogen molecules in the system and the symbol F_{fpn} denotes the average resultant force on each atom of nitrogen molecules by fuel molecules in this paper. It is worth noting that all fuel components are now considered as a whole, rather than distinguishing individual components. Figures 13-14 show the curves of F_{npfa} and F_{fpn}, respectively. As shown in Figure 13, no matter what kind of fuel, when the ambient pressure remains constant and the ambient temperature increases, F_{npfa} will increase at the same time. Similarly, F_{npfa} will also increase with increasing pressure at constant temperature. As shown in Figure 14, when the ambient pressure or temperature increases, F_{fpn} will increase at the same time. The consistency of the profile tendencies of Figures 13 and 14 is the inevitable result of Newton's third law. Moreover, F_{fpn} in the single-component droplet system is the

largest among that of three fuel droplet systems under the same environmental conditions at the same time, which relies on the number and type of fuel atoms that nitrogen interacts with at a certain moment.

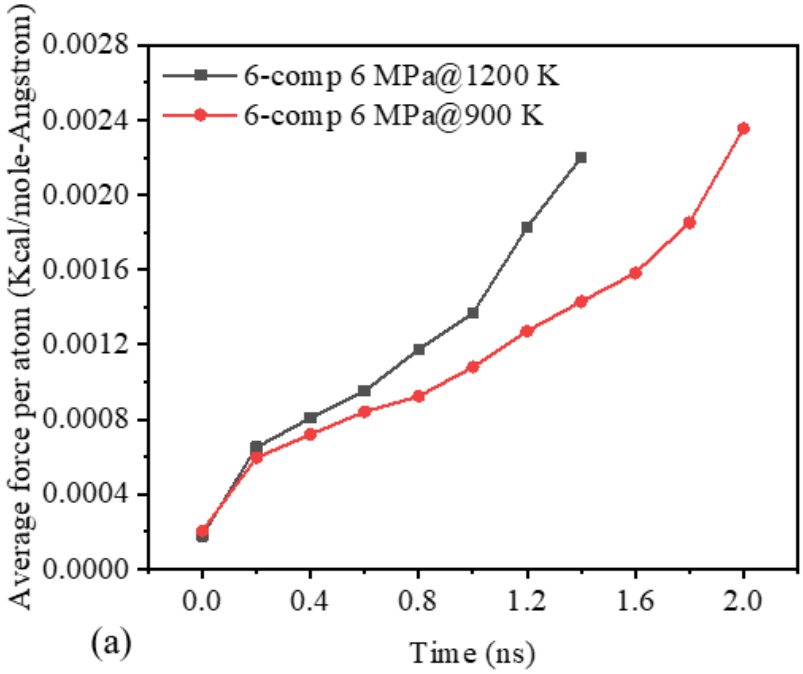

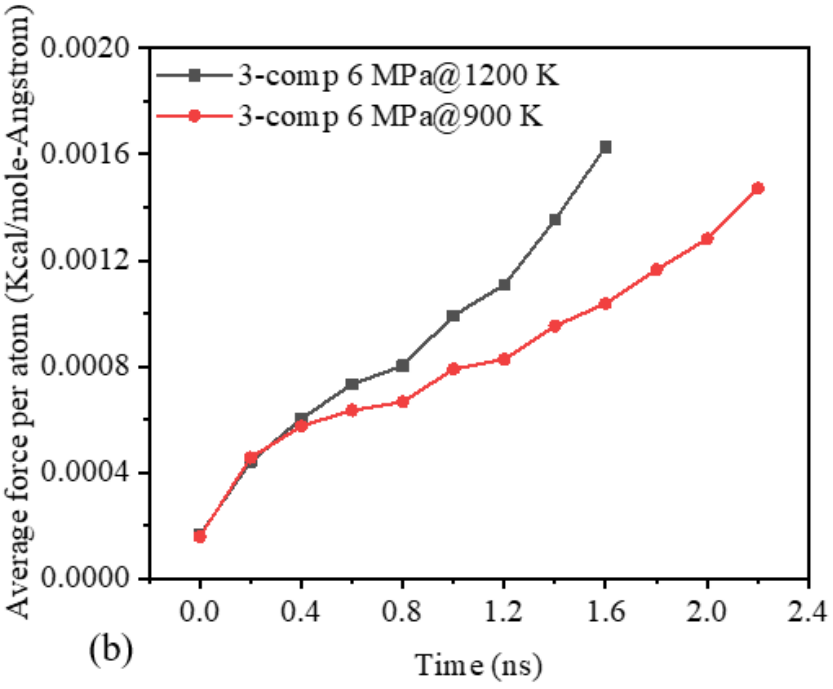

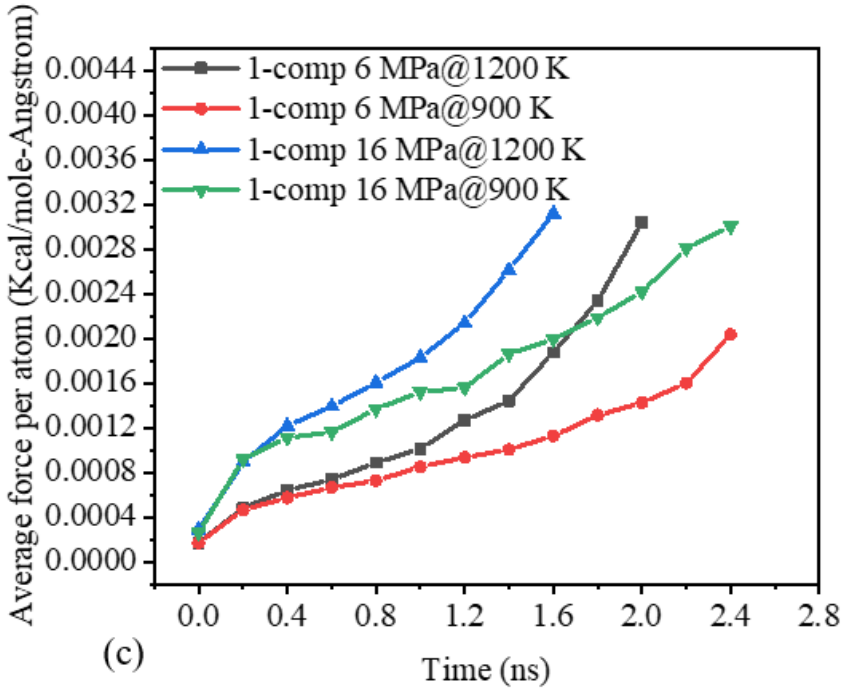

451

452 **Fig. 13.** Average resultant force on each atom of fuel droplets by nitrogen molecules: (a) Six-component

453 droplet, (b) Three-component droplet, and (c) Single-component droplet.

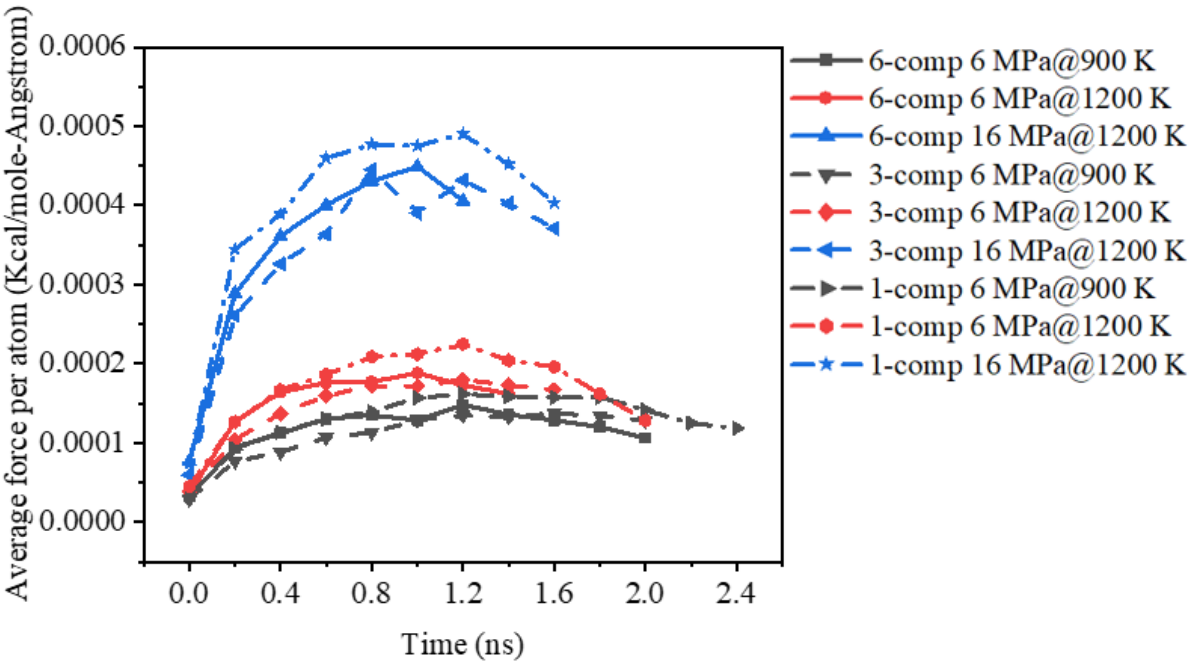

454

455 **Fig. 14.** Average resultant force on each atom of nitrogen molecules by fuel molecules.

The interaction between nitrogen molecules and fuel molecules can also be discussed from the perspective of molecular energy of the mixed fuel. Figure 15 shows the average energy per fuel atom of six-component fuel droplets under different ambient conditions. The per-atom translational kinetic energy or potential energy for fuel atoms increases with increasing ambient temperature at a certain moment, as shown in Figure 15a. A special attention should be paid here. The 12-6 Lennard-Jones pair potential energy between atoms here is always negative, which is only a part of the overall potential energy of fuel atoms. In fact, the overall potential energy of fuel atoms is positive, as shown in Figure 15. The fuel-ambient gas mixing accelerates with increasing temperature, and the pair potential energies of fuel molecules increases in value with increasing intermolecular distances at the same time, causing the increasing overall potential energy. When the temperature remains constant and the pressure increases, the per-atom translational kinetic energy for fuel atoms increases due to the increasing number density of nitrogen molecules with the average translational kinetic energy of nitrogen molecules remaining constant, as shown in Figure 15b. The whole interaction between nitrogen molecules and fuel molecules strengthens at a certain moment, and the energy transfer rate between them increases, which is consistent with Figure 14. The per-atom potential energy for fuel atoms also increases with increasing pressure, as shown in Figure 15b. At higher pressure, more nitrogen molecules diffuse into the droplet within the same time, as shown in Figure 6. The number of nitrogen molecules around each fuel atom increases (See more details in Fig. 17), and that part of fuel per-atom pair potential energy deriving from the interactions with nitrogen atoms rapidly decreases in value (See more details in Fig. 19). Although the mean square displacement (MSD) of each component decreases (See more details in Fig. 16), the pair potential energy between fuel molecules increases in value at a certain time, which will be discussed in detail later (Fig. 19). Due to the change of pair potential energy between fuel molecules exceeding that between fuel molecules and nitrogen molecules, the pair potential energy of fuel atoms increases in value, resulting in the increasing potential energy for fuel atoms. The per-atom translational kinetic energy for fuel atoms also increases

480 with time due to the increasing fuel temperature. Meanwhile, the per-atom potential energy for fuel atoms
481 increases due to the increasing intermolecular distance with time.

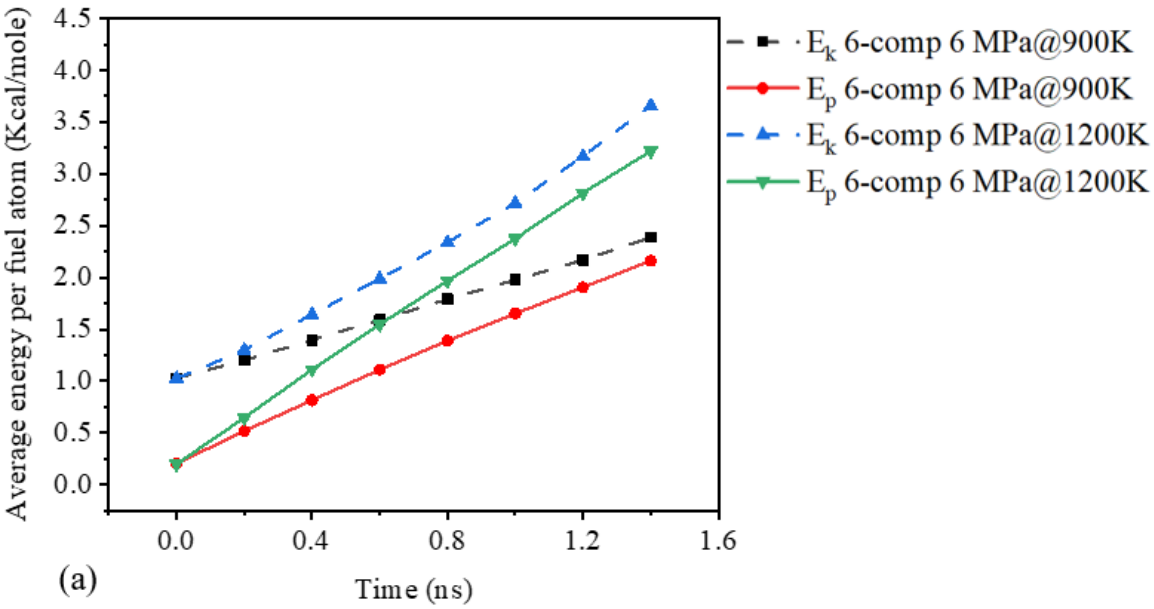

482

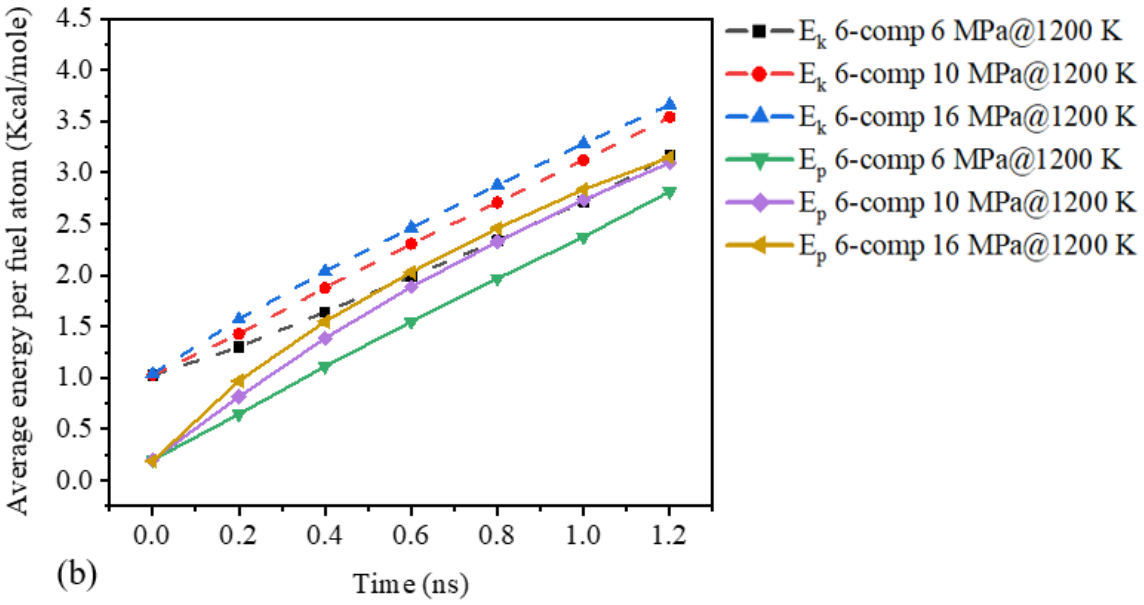

483

484 **Fig. 15.** Average energy per fuel atom of six-component fuel droplets: (a) 6 MP and (b) 1200 K.

485 Figure 16 shows the MSD of the methyl group (CH_3) of n-hexadecane in 6-component droplets under
486 different environmental conditions. When the ambient pressure remains constant and the ambient
487 temperature decreases, as the average translational kinetic energy of nitrogen molecules decreases and the

number density of them increases, the diffusion of fuel molecules into the ambient gas becomes slower. When the ambient temperature remains unchanged and the ambient pressure increases, the average translational kinetic energy of nitrogen molecules remains unchanged, but the number density of them increases, and the diffusion of fuel molecules into the ambient gas also slows down. It should be noted that the discussion here is focused on the movement of fuel molecules. The fuel-ambient gas mixing is also related to the diffusion of nitrogen molecules into fuel droplets, which has been discussed before.

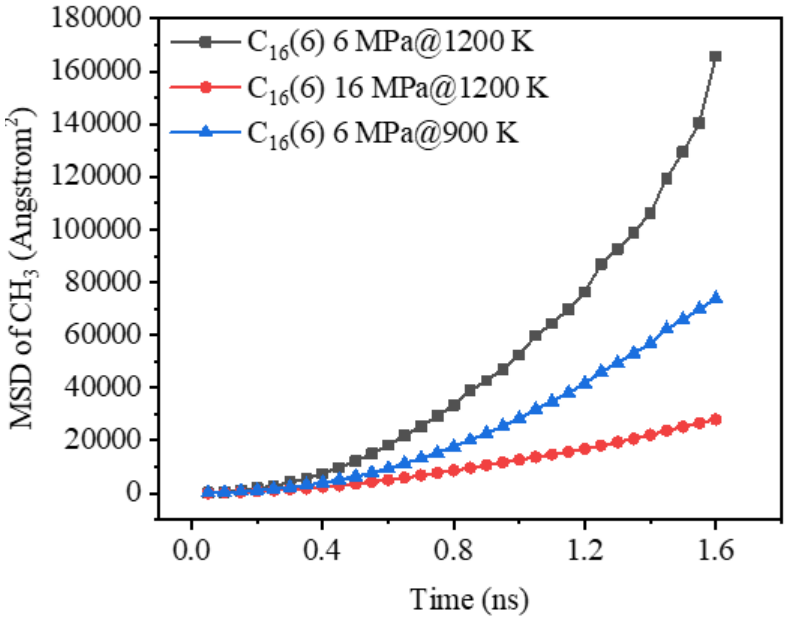

Fig. 16. MSD of CH_3 of n-hexadecane in six-component fuel droplets.

Figure 17 shows the coordination number curve of the methyl and nitrogen molecules (CH_3-N_2) of toluene molecules, n-dodecane molecules and n-hexadecane molecules in a six-component fuel droplet at a certain time (t = 1.2 ns) during the mixing process. The methyl group is the central atom and the nitrogen molecules are distributed around it. As shown in Figure 17, the number of nitrogen molecules around the methyl group of the fuel molecule increases with increasing pressure or decreasing temperature. The coordination profile is not only related to the evaporation rate of the droplets, but also to the number density and average translational kinetic energy of the nitrogen molecules. At a certain radial distance, to a certain extent, the fuel-ambient gas mixing becomes more complete with higher coordination number of

CH_3-N_2. In addition, as shown in Figure 6, the time chosen in this figure (t = 1.2 ns) is near the end of the evaporation process, which means the mixing has been fully developed. Figure 17 shows that for the coordination number of CH_3-N_2 at a certain moment, n-hexadecane > n-dodecane > toluene. The conclusion could be drawn that in the case of fully developed mixing, there are more nitrogen molecules around the methyl groups of the long-chain molecules.

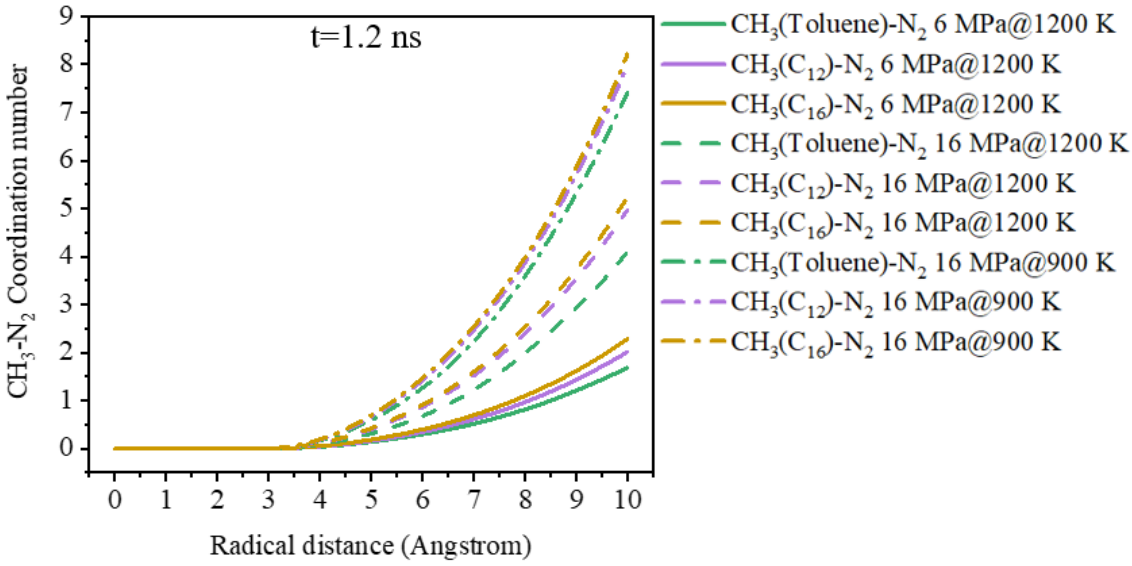

Fig. 17. Coordination number profiles of CH_3-N_2 in six-component fuel droplets.

Figure 18 shows the ratio of interactive force of representative component and that of pair potential energy of representative component in the six-component fuel droplet system under constant pressure. To simplify discussions, n-decane was chosen to represent the light component, and n-hexadecane was chosen to represent the heavy component here. Moreover, it is worth mentioning that the interactive force from the 12-6 Lennard-Jones potential between molecules is always a negative value under the conditions investigated here. Because of this, the following discussions on intermolecular forces are about their absolute values. As seen from Figure 18a, when the ambient pressure remains unchanged and the ambient temperature increases, the ratio of the interaction force between n-decane and several fuel components, such as dodecane, is less than 1 at the initial stage of evaporation (t < 0.3 ns). However, at all moments

when the evaporation time $t \geq 0.3$ ns, the ratio of the interaction force between n-decane and all other fuel components exceeds 1, which means the internal force of the fuel components decreases with increasing temperature at constant pressure. The case of n-hexadecane is similar to that of n-dodecane, as shown in Figure 18c. At the initial stage of evaporation ($t < 0.2$ ns), except the interactive pair of n-octadecane and n-hexadecane, the ratio of the interaction force between n-hexadecane and all other fuel components exceeds 1. At all moments when the evaporation time $t \geq 0.2$ ns, the ratio of the interaction force between n-hexadecane and all other fuel components always exceeds 1, which means the internal force of the fuel components decreases, consistent with the case of n-decane. On the whole, the internal force of the fuel components will decrease at all moments after a short initial mixing with increasing temperature under constant pressure. As for the pair potential energy between the components, as shown in Figures 18b and 18d, during the fuel–ambient gas mixing process, the potential energy of all fuel components at all moments will increase in value with increasing temperature at constant pressure. As mentioned before, the pair potential energy is always negative in value, so its absolute value will decrease. In addition, after the evaporation time $t > 0.6$ ns, the ratio profile increases almost exponentially with time.

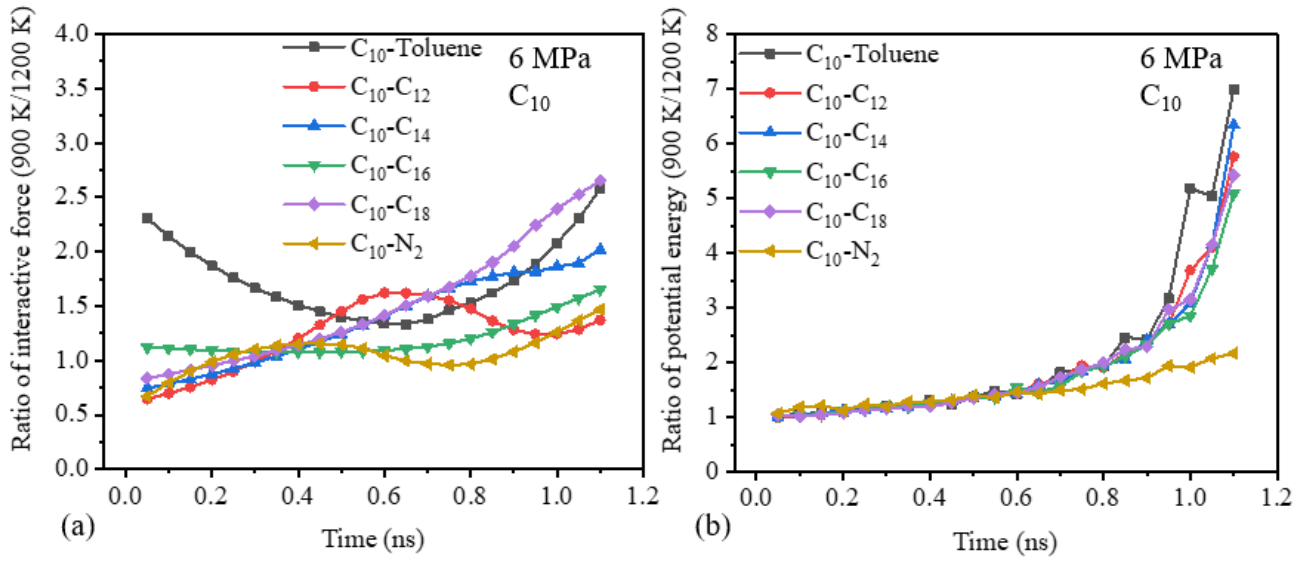

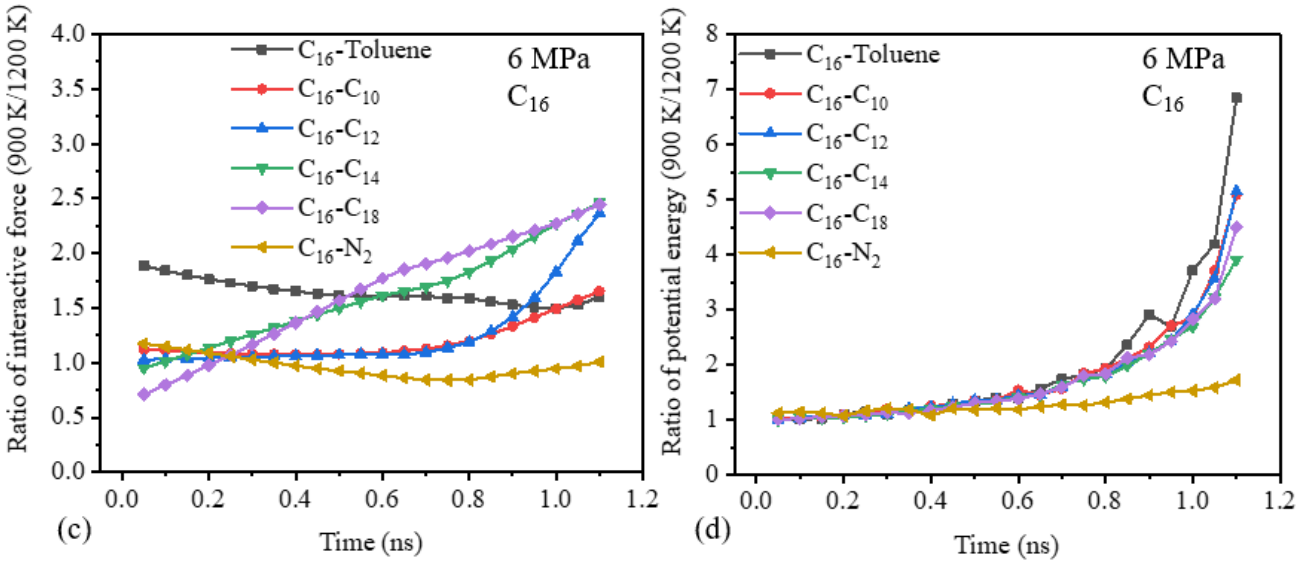

Fig. 18. Ratio of interactive force of representative component and pair potential energy of representative component in the six-component fuel droplet system under constant pressure: (a) Interactive force on n-decane, (b) Pair potential energy of n-decane, (c) Interactive force on n-hexadecane and (d) Pair potential energy of n-hexadecane.

Figure 19 shows the ratio of interactive force of representative component and that of pair potential energy of representative component in the six-component fuel droplet system under constant temperature. As seen from Figure 19a, when the ambient temperature remains unchanged and the ambient pressure increases, almost all of the time in the whole mixing process, the ratio of the interaction force between n-decane and all other fuel components exceeds 1, which means the internal force of the fuel components decreases with increasing pressure at constant temperature. The case of n-hexadecane is similar to that of n-dodecane, as shown in Figure 19c. At the early stage of evaporation ($t < 0.55$ ns), except the interactive pair of n-hexadecane and n-tetradecane, the ratio of the interaction force between n-hexadecane and all other fuel components exceeds 1. At all moments when the evaporation time $t \geq 0.55$ ns, the ratio of the interaction force between n-hexadecane and all other fuel components always exceeds 1, which means the internal force of the fuel components decreases, consistent with the case of n-decane. On the whole, the internal force of the fuel components will decrease with increasing pressure at constant temperature. The

following discussion will be focused on the pair potential energy between the components. As shown in Figures 19b and 19d, during the fuel-ambient gas mixing process, the potential energy of all fuel components at all moments will increase in value with increasing pressure at constant temperature and its absolute value will decrease. Moreover, during the whole mixing time, the ratio profile of potential energy increases almost linearly with time, which is different from the case shown in Figure 18.

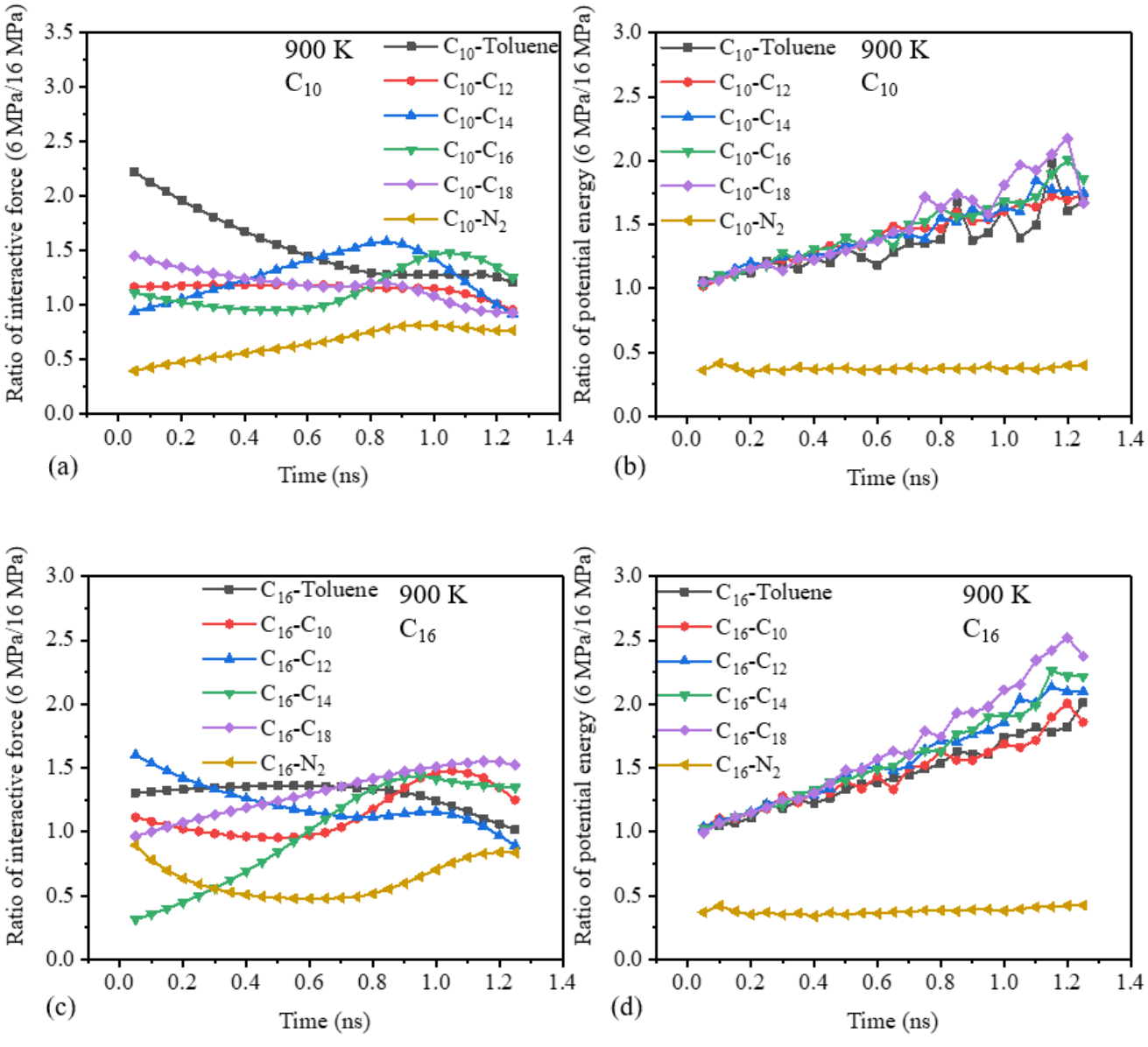

Fig. 19. Ratio of interactive force of representative component and pair potential energy of representative component in the six-component fuel droplet system under constant temperature: (a)

Interactive force on n-decane, (b) Pair potential energy of n-decane, (c) Interactive force on n-hexadecane and (d) Pair potential energy of n-hexadecane.

3.3.2 Atomic-level insights into the clustering phenomenon of fuel droplet system

According to previous reports [71, 72], clusters are likely to form in supercritical fluids. Because the fuel droplets studied in this paper have a transition of the dominant mixing mode under supercritical conditions, it is expected that fuel clusters will form during the mixing process. In order to investigate the cluster formation during fuel-ambient gas mixing, the size distributions of CH_3 clusters for single-component n-hexadecane droplet evaporation under different environmental conditions are shown in Figure 20. The discussion here is focused on the clusters of CH_3 groups on the fuel molecules. Moreover, only large clusters containing at least 10 CH_3 groups are considered for statistical analysis here. With reference to the previously reported researches [73], the cutoff distance of the cluster was chosen as 8 angstroms. The moment chosen here to calculate the cluster rate is the vapor–liquid equal probability time $t_{pv=pl}$ proposed in the previous study [9]. As seen from Figure 20a-b, under the ambient condition of 6 MPa and 900 K, the largest fuel clusters appearing in the evaporation system contain more than 30 CH_3 groups. 33.6% of the total CH_3 groups leaving the droplet were contained in clusters containing more than 20 CH_3 groups. When the ambient temperature rises to 1200 K, the largest cluster contains less than 30 methyl groups, and only 7.48% of the total CH_3 groups leaving the droplet were contained in clusters containing more than 20 CH_3 groups. In other words, with increasing ambient temperature at constant pressure, the size of the largest clusters in the evaporation system decreases, and the proportion of large clusters in the evaporation system decreases. As seen from Figure 20c-f, at higher ambient pressure, when the ambient temperature rises, the formation mechanisms of clusters are similar. Under the condition of 900 K and 16 MPa, the largest fuel cluster appearing in the evaporation system contains more than 50 methyl groups. 29.83% of the total CH_3 groups leaving the droplet were contained in clusters containing more than 30 CH_3 groups. While at 6 MPa, this proportion is only 8.53%, as shown in Figures 20a and

20e. In summary, with increasing ambient pressure at constant temperature, the size of the largest cluster in the evaporation system increases, and the proportion of large clusters in the evaporation system increases.

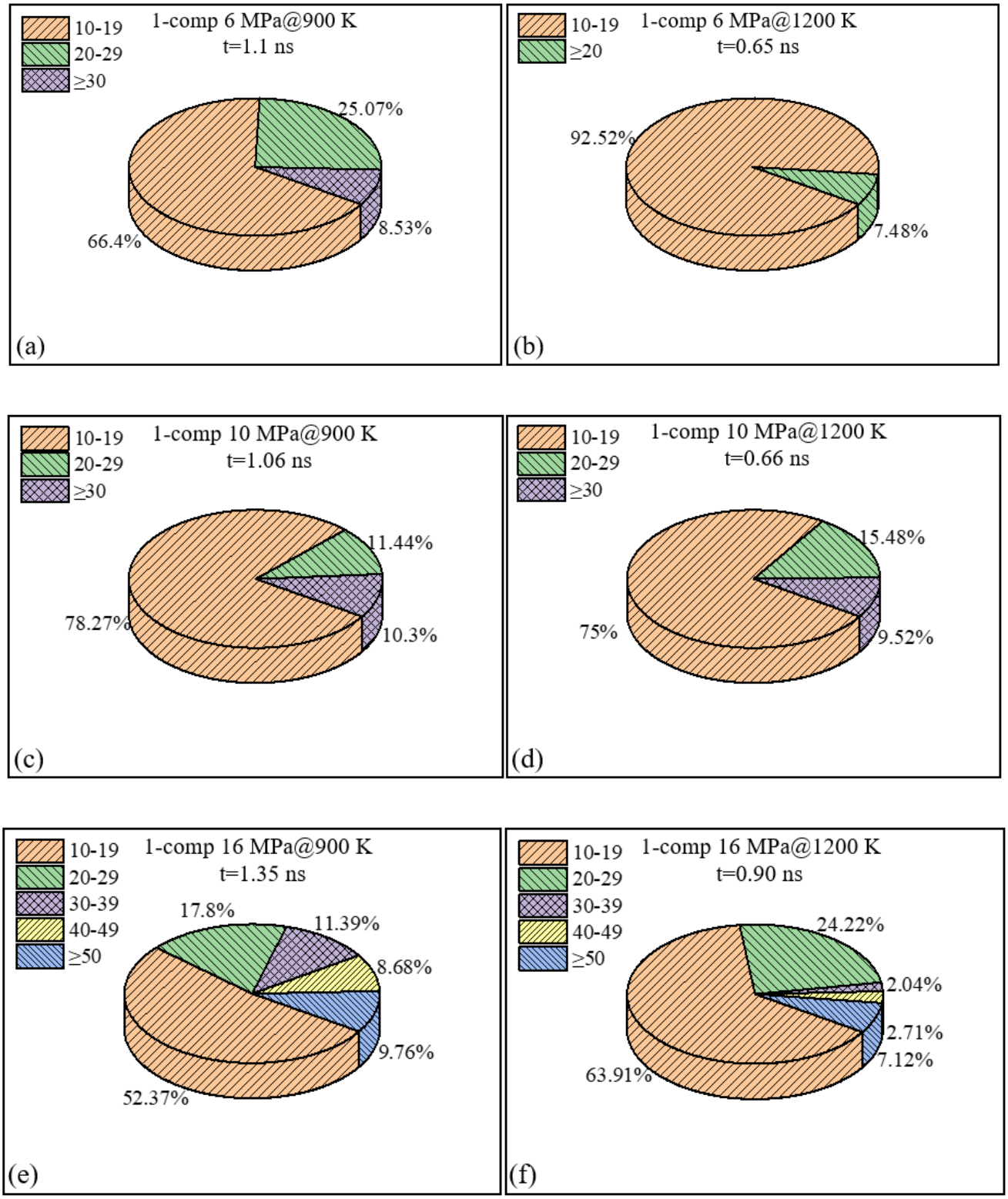

Fig. 20. Size distributions of CH_3 clusters (cut-off distance = 8 angstroms) for single-component droplet evaporation under different ambient conditions: (a) 6 MPa and 900 K, (b) 6 MPa and 1200 K, (c) 10 MPa and 900 K, (d) 10 MPa and 1200 K, (e) 16 MPa and 900 K and (f) 16 MPa and 1200 K.

Figure 21 shows the cluster rate of CH_3 and the equal probability time of vapor-liquid phase $t_{pv=pl}$ during the mixing process of fuel droplets under different environmental conditions. As seen from Figure 21a, under the same working conditions, when $t_{pv=pl}$, the cluster rate of the six components is the lowest. This is because the relative molecular mass of the six-component fuel is the lowest, which means its content of the light component is the highest among three fuels. The average kinetic energy of the molecules of the light components is larger, as shown in Figure 9. Therefore it is not easy for this six-component fuel to form clusters; while the average kinetic energy of the molecules of the heavy components is smaller, and the molecular chain is longer, the force between the molecules is greater, so it is easier for them to form clusters. The relative molecular mass of the three-component droplets is centered among the three fuels, and its cluster rate is also centered among the three fuels. The relative molecular mass of single-component droplets is the largest, so the cluster rate of single-component droplets is the highest. As shown in Figure 21a, under the supercritical temperature conditions studied in this paper, when the ambient pressure remains unchanged and the ambient temperature rises, the cluster rate decreases. This is because when the environmental pressure is constant, the average kinetic energy of N_2 molecules increases with increasing temperature, and the average kinetic energy of fuel molecules also increases, so it is not easy to form clusters. When the ambient temperature remains unchanged and the ambient pressure increases, the cluster rate increases. This is because the MSD of the fuel molecules decreases and the dissolution of nitrogen increases. The liquid fuel is disintegrated into smaller clumps and the mixing is dominated by diffusion, so the clustering rate is high. Under the same environmental conditions, as for $t_{pv=pl}$, the 1-component droplet is the largest, the 3-component droplet is second, and the 6-component droplet is the smallest, as shown in Figure 21b. The smaller relative molecular mass of

615 the mixed fuel, the higher the content of light components and the faster the mixing, so $t_{pv=pl}$ is smaller.
616 The fuel evaporates faster with increasing ambient temperature, and $t_{pv=pl}$ is smaller. However, the
617 influence of pressure on the evaporation rate is more complicated. As diffusion dominates the fuel-ambient
618 gas mixing process instead of evaporation, the dominant factor of the mixing rate changes, the profile of
619 $t_{pv=pl}$ with increasing ambient pressure is not monotonous.

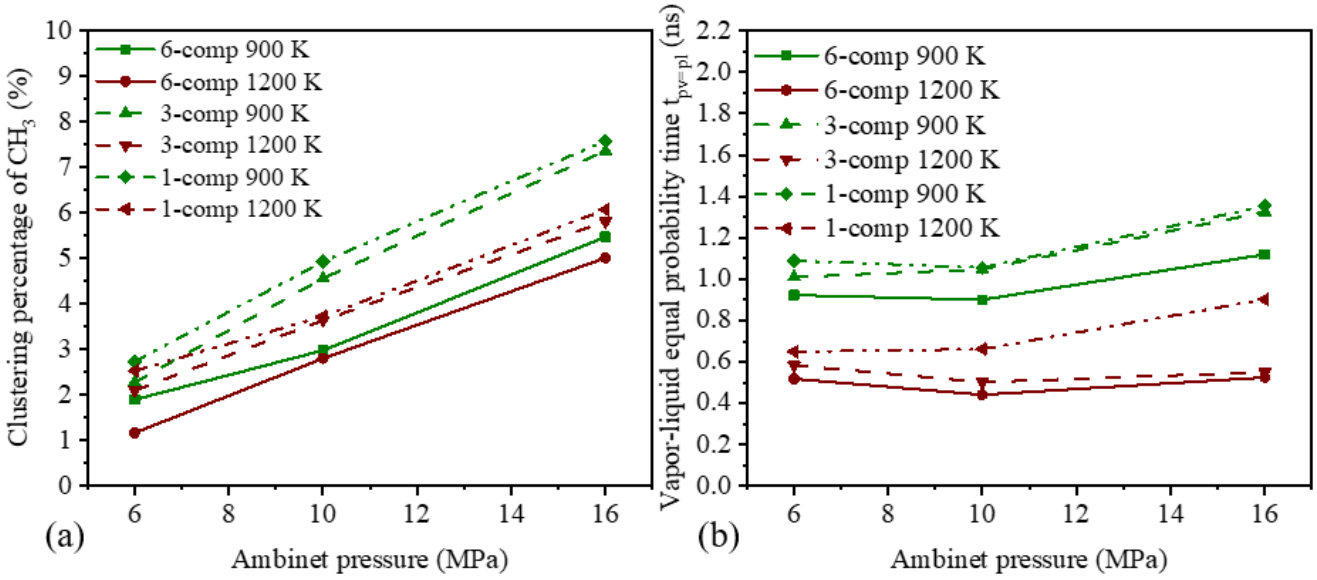

620

621 **Fig. 21.** Clustering of CH_3 (cut-off distance=8 angstrom) during the mixing process of fuel droplets
622 under different ambient conditions: (a) Cluster ratio at $t_{pv=pl}$ and (b) Vapor-liquid equal probability time
623 $t_{pv=pl}$.

624 Figure 22 shows the snapshots of local molecular distributions of six-component fuel droplets.
625 According to the classification of Figure 4a, Figures 22a and 22b respectively show the snapshots of
626 distribution of fuel molecules when the fuel droplets are in diffusion mode and evaporation mode. In order
627 to show the phase change process of fuel more clearly, nitrogen molecules are not shown. The moment of
628 the snapshot here is the vapor–liquid equal probability time $t_{pv=pl}$. When the mixing process of fuel
629 droplets is dominated by diffusion, a large number of nitrogen molecules dissolve into the inside of the
630 droplets. The existing vapor-liquid interface gradually collapses, and the fuel disintegrates into a large

number of clumpy clouds in the mixing layer, forming potential fuel clusters, as shown in Figure 22a. When evaporation dominates the mixing process of fuel droplets, although there is still dissolved nitrogen in the droplets, it is not enough to break the gas-liquid interface, so it is difficult to form fuel clusters, as shown in Figure 22b. In Figure 22c, in order to show the dissolution of nitrogen molecules inside the fuel droplets, fuel molecules and nitrogen molecules are displayed at the same time. When diffusion dominates the fuel-ambient gas mixing process, a large number of nitrogen molecules dissolve into the fuel. In order to visually show the process, a slice through the center of the droplet when the fuel droplet is in diffusion mode is shown here, as shown in Figure 22c. It can be seen from the figure that a large number of nitrogen molecules are dissolved inside the droplet, and the gas-liquid interface of the droplet has been disintegrating, so nitrogen enters the droplet more easily, and the droplet disintegrates from the inside, which is beneficial to form fuel clusters. Two representative clusters are shown in Figs. 22d and e, respectively. In Fig. 22d-e, only CH_3 groups are shown here and different CH_3 clusters are represented with different colors. The largest cluster colored in green is the remaining fuel droplet, which has been omitted in the statistical analysis of clusters. If a particle does not find neighbors within the cutoff distance, it will be identified as a cluster with only one particle. It can be found that fuel clusters form in the fuel-ambient gas mixing layer where the dominant mixing mode transition happens.

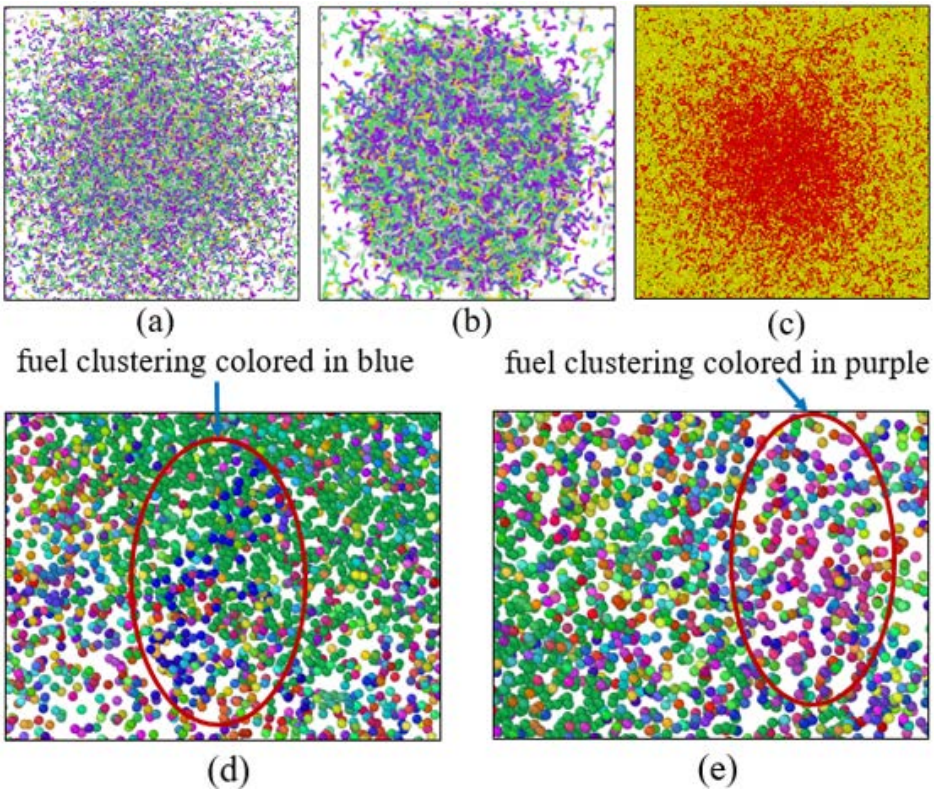

Fig. 22. Snapshots of local molecular distributions of six-component fuel droplets: (a) Diffusion mode (16 MPa and 900 K, t = 1.12 ns), (b) Evaporation mode (2 MPa and 750 K, t = 1.75 ns), (c) A slice through the droplet center (16 MPa and 900 K, t = 1.12 ns), (d) Representative cluster colored in blue (16 MPa and 900 K, t = 1.12 ns) and (e) Representative cluster colored in purple (16 MPa and 900 K, t = 1.12 ns). In Fig. 22a-b, blue particles indicate toluene molecules, yellow particles n-decane molecules, purple particles n-dodecane molecules, green particles n-tetradecane molecules, dark blue particles n-hexadecane molecules and grey particles n-octadecane molecules. Nitrogen molecules are not shown here. In Fig. 22c, red particles indicate fuel molecules and yellow particles indicate nitrogen molecules.

4. Conclusions

The evaporation processes of six-component hydrocarbon fuel droplets in nitrogen environments were studied using MD simulations. As a comparison, three-component droplet and pure n-hexadecane droplet evaporation processes were also studied. The ambient pressure ranged from 2 MPa to 16 MPa and

660 the ambient temperature ranged from 750 K to 1350 K, which cover both subcritical and supercritical
661 regimes. Significant results of this study include:

662 1) The transition characteristics of the mixed fuel are strongly related to the interactive forces between the
663 fuel molecules. And the properties of the mixed fuel are not the weighted average of those of individual
664 fuel components. Therefore, the transition characteristics of the mixed fuel would not be the linearly
665 weighted average of the physical properties of individual components in the mixture based on the mole
666 fraction. The transition of a certain component in the mixed fuel will be affected by other components.
667 For a certain pure component in the mixed fuel, the minimum transition pressure of it at certain
668 temperature will increase with the decreasing relative molecular mass of the mixed fuel. The number of
669 nitrogen molecules dissolved into the droplet decreases with increasing temperature even at the
670 supercritical pressure condition, which is the reason why there is a limitation namely the maximum
671 transition temperature.

672 2) For the same mixed fuel evaporation system (the same mixed fuel and the same ambient gas) at the
673 supercritical temperature, F_{pfa} increases with increasing pressure at constant temperature (The symbol F_{pfa}
674 denotes the average resultant force on each atom of an individual component in mixed fuel droplets by all
675 the other atoms in the system). As a result, diffusion will gradually dominate the mixing process of the
676 component. However, F_{pfa} will decrease with increasing temperature at constant pressure. Consequently,
677 evaporation will gradually dominate the mixing process of the component. For a certain pure component,
678 F_{pfa} is different in different mixed systems, resulting in its different transition points. When the ambient
679 pressure or temperature increases, F_{npfa} will increase at the same time (The symbol F_{npfa} denotes the
680 average resultant force on each fuel atom by nitrogen molecules in the system). The per-atom translational
681 kinetic energy or potential energy for fuel atoms increases with increasing temperature or pressure. The
682 MSD of fuel molecules decreases with the ambient pressure increasing or the ambient temperature
683 decreasing at the same time. In the case of fully developed mixing, there are more nitrogen molecules

around the methyl groups of the long-chain molecules. On the whole, the internal force of the fuel components will decrease with increasing pressure or temperature. Moreover, the potential energy of all fuel components at all moments will always increase in value with increasing pressure or temperature and its absolute value will decrease. During the whole mixing time, in the case of varying pressure, the ratio profile (low-pressure case/high-pressure case) of potential energy of fuel components increases almost linearly with time. However, in the case of varying temperature, the ratio profile (low-temperature case/high-temperature case) increases almost exponentially with time at the later stage of mixing.

3) In the case of supercritical temperature studied here, with increasing ambient temperature at constant pressure, the size and the proportion of large clusters in the evaporation system as well as the cluster rate all decrease. When increasing pressure at constant temperature, the situations are just the opposite. Under the same working conditions, at $t_{pv=pl}$ ($t_{pv=pl}$ denotes the vapor-liquid equal probability time), the smaller the relative molecular mass of the mixed fuel is, the lower its cluster rate is. Fuel clusters form in the fuel-ambient gas mixing layer where the dominant mixing mode transition happens.

Acknowledgements

Support from the Natural Science Foundation of China (Grant No. 51976100) and the UK Engineering and Physical Sciences Research Council under the project “UK Consortium on Mesoscale Engineering Sciences (UKCOMES)” (Grant No. EP/R029598/1) is gratefully acknowledged.

References

[1] Ju D, Deng J, Huang Z, Xia J, Qin H, Jiang F. Large Eddy Simulation with dense fluid approximation and experimental study on the commercial diesel trans-critical injections. Applied Thermal Engineering 2021;183. https://doi.org/10.1016/j.applthermaleng.2020.116181.

[2] Huang Z, Zhang W, Xia J, Ju D, Lu X. A multi-component surrogate of commercial diesel for trans-critical and supercritical injections study. Fuel 2019;243:590-602. https://doi.org/10.1016/j.fuel.2019.01.162.

[3] Rowane AJ, Gupta A, Gavaises M, McHugh MA. Experimental and modeling investigations of the phase behavior and densities of diesel + nitrogen mixtures. Fuel 2020;265. https://doi.org/10.1016/j.fuel.2020.117027.

[4] Xiao G, Luo KH, Ma X, Shuai S. A molecular dynamics study of fuel droplet evaporation in sub- and supercritical conditions. Proceedings of the Combustion Institute 2019;37(3):3219-27. https://doi.org/10.1016/j.proci.2018.09.020.

[5] Dahms RN, Manin J, Pickett LM, Oefelein JC. Understanding high-pressure gas-liquid interface phenomena in Diesel engines. Proceedings of the Combustion Institute 2013;34(1):1667-75. http://dx.doi.org/10.1016/j.proci.2012.06.169.

[6] Ashraf C, Shabnam S, Xuan Y, van Duin ACT. Application of ReaxFF-Reactive Molecular Dynamics and Continuum Methods in High-Temperature/Pressure Pyrolysis of Fuel Mixtures. Computational Approaches for Chemistry Under Extreme Conditions. 2019, p. 161-85. https://doi.org/10.1007/978-3-030-05600-1_7.

[7] Poursadegh F, Lacey J, Brear M, Gordon R. The Direct Transition of Fuel Sprays to the Dense-Fluid Mixing Regime in the Context of Modern Compression Ignition Engines. *SAE Technical Paper Series.* 2018. https://doi:10.4271/2018-01-0298.

[8] Poursadegh F, Lacey JS, Brear MJ, Gordon RL. On the Fuel Spray Transition to Dense Fluid Mixing at Reciprocating Engine Conditions. Energ Fuel 2017;31(6):6445-54. https://doi:10.1021/acs.energyfuels.7b00050.

[9] Gong Y, Xiao G, Ma X, Luo KH, Shuai S, Xu H. Phase transitions of multi-component fuel droplets under sub- and supercritical conditions. Fuel 2021;287(119516). https://doi.org/10.1016/j.fuel.2020.119516.

[10] Crua C, Manin J, Pickett LM. On the transcritical mixing of fuels at diesel engine conditions. Fuel 2017;208:535-48. http://dx.doi.org/10.1016/j.fuel.2017.06.091.

[11] Manin J, Bardi M, Pickett LM, Dahms RN, Oefelein JC. Microscopic investigation of the atomization and mixing processes of diesel sprays injected into high pressure and temperature environments. Fuel 2014;134:531-43. http://dx.doi.org/10.1016/j.fuel.2014.05.060.

[12] Falgout Z, Rahm M, Wang Z, Linne M. Evidence for supercritical mixing layers in the ECN Spray A. Proceedings of the Combustion Institute 2015;35(2):1579-86. http://dx.doi.org/10.1016/j.proci.2014.06.109.

[13] Dahms RN, Oefelein JC. On the transition between two-phase and single-phase interface dynamics in multicomponent fluids at supercritical pressures. Phys Fluids 2013;25(9):092103-27. https://doi.org/10.1063/1.4820346.

[14] Xia J, Zhang Q, Huang Z, Ju D, Lu X. Experimental study of injection characteristics under diesel's sub/trans/supercritical conditions with various nozzle diameters and injection pressures. Energ Convers Manage 2020;215:112949-60. https://doi.org/10.1016/j.enconman.2020.112949.

[15] Zhan C, Tong S, Tang C, Huang Z. The spray vaporization characteristics of gasoline/diethyl ether blends at sub-and super-critical conditions. Applied Thermal Engineering 2020;164:114453-65. https://doi.org/10.1016/j.applthermaleng.2019.114453.

[16] Zhang Q, Xia J, He Z, Wang J, Liu R, Zheng L, et al. Experimental study on spray characteristics of six-component diesel surrogate fuel under sub/trans/supercritical conditions with different injection pressures. Energy 2021;218. https://doi.org/10.1016/j.energy.2020.119474.

[17] Liu F, Gao Y, Zhang Z, He X, Wu H, Zhang C, et al. Study of the spray characteristics of a diesel surrogate for diesel engines under sub/supercritical states injected into atmospheric environment. Fuel 2018;230:308-18. https://doi.org/10.1016/j.fuel.2018.05.050.

[18] Kitano T, Nishio J, Kurose R, Komori S. Evaporation and combustion of multicomponent fuel droplets. Fuel 2014;136:219-25. http://dx.doi.org/10.1016/j.fuel.2014.07.045.

[19] Millán-Merino A, Fernández-Tarrazo E, Sánchez-Sanz M. Theoretical and numerical analysis of the evaporation of mono- and multicomponent single fuel droplets. J Fluid Mech 2021;910. doi:10.1017/jfm.2020.950.

[20] Sazhin SS. Modelling of fuel droplet heating and evaporation: Recent results and unsolved problems. Fuel 2017;196:69-101. http://dx.doi.org/10.1016/j.fuel.2017.01.048.

[21] Banuti DT, Raju M, Ihme M. Between supercritical liquids and gases – reconciling dynamic and thermodynamic state transitions. The Journal of Supercritical Fluids 2020;165:104895-900. https://doi.org/10.1016/j.supflu.2020.104895.

[22] Simeoni GG, Bryk T, Gorelli FA, Krisch M, Ruocco G, Santoro M, et al. The Widom line as the crossover between liquid-like and gas-like behaviour in supercritical fluids. Nature Physics 2010;6(7):503-7. DOI: 10.1038/NPHYS1683.

[23] Wensing M, Vogel T, Gotz G. Transition of diesel spray to a supercritical state under engine conditions. International Journal of Engine Research 2015;17(1):108-19. DOI: 10.1177/1468087415604281.

[24] Yi P, Li T, Fu Y, Xie S. Transcritical evaporation and micro-explosion of ethanol-diesel droplets under diesel engine-like conditions. Fuel 2021;284. https://doi.org/10.1016/j.fuel.2020.118892.
[25] He R, Yi P, Li T. Evaporation and condensation characteristics of n-heptane and multi-component diesel droplets under typical spray relevant conditions. Int J Heat Mass Tran 2020;163. https://doi.org/10.1016/j.ijheatmasstransfer.2020.120162.
[26] Shawn D. Givler JA. Supercritical Droplet Vaporization and Combustion Studies. Progress in Energy and Combustion Science 1996;22:1-28.
[27] Bellan J. Supercritical (and subcritical) fluid behavior and modeling: drops, streams, shear and mixing layers, jets and sprays. Progress in Energy and Combustion Science 2000;26:329–66.
[28] Yang V. Modeling of supercritical vaporation,mixing,and combustion process in liquid-fueled processes in liquid-fueled propulsion systems. Proceedings of the Combustion Institute 2000;28:925–42.
[29] Chiu HH. Advances and challenges in droplet and spray combustion. I. Toward a unified theory of droplet aerothermochemistry. Progress in Energy and Combustion Science 2000;26:381–416.
[30] Xiao G, Luo KH, Ma X, Shuai S. Liquid Fuel Evaporation under Supercritical Conditions. Commun Comput Phys 2018;23(4):1241-62. doi: 10.4208/cicp.OA-2016-0252.
[31] Stubbs JM. Molecular simulations of supercritical fluid systems. The Journal of Supercritical Fluids 2016;108:104-22. http://dx.doi.org/10.1016/j.supflu.2015.10.027.
[32] Nasiri R, Luo KH. Specificity Switching Pathways in Thermal and Mass Evaporation of Multicomponent Hydrocarbon Droplets: A Mesoscopic Observation. Sci Rep 2017;7(1):5001. DOI:10.1038/s41598-017-05160-z.
[33] Ma Z, Li Y, Li Z, Du W, Yin Z, Xu S. Evaporation and combustion characteristics of hydrocarbon fuel droplet in sub- and super-critical environments. Fuel 2018;220:763-8. https://doi.org/10.1016/j.fuel.2018.02.073.
[34] Nomura H, Murakoshi T, Suganuma Y, Ujiie Y, Hashimoto N, Nishida H. Microgravity experiments of fuel droplet evaporation in sub- and supercritical environments. Proceedings of the Combustion Institute 2017;36(2):2425-32. http://dx.doi.org/10.1016/j.proci.2016.08.046.
[35] Ghassemi H, Baek SW, Khan QS. Experimental Study on Binary Droplet Evaporation at Elevated Pressures and Temperatures. Combust Sci Technol 2006;178(6):1031-53. https://doi.org/10.1080/00102200500296697.
[36] Seo J, Lee S, Kim H. Measurement and correlation of vapor-liquid equilibria for the ethanol plus n-heptane system near the critical region. J Chem Eng Data 2002;47(4):974-7.

[37] Yang S. Towards a multicomponent real-fluid fully compressible two-phase flow model. 2018.
[38] Yang S, Yi P, Habchi C. Real-fluid injection modeling and LES simulation of the ECN Spray A injector using a fully compressible two-phase flow approach. Int J Multiphas Flow 2020;122. https://doi.org/10.1016/j.ijmultiphaseflow.2019.103145.
[39] Wang Z, Zhou L, Shu G, Wei H. Droplet evaporation and phase transition modes in supercritical environment by molecular dynamic simulation. Phys Fluids 2021;33(6). https://doi.org/10.1063/5.0053328.
[40] Rahmani F, Weathers T, Hosangadi A, Chiew YC. A non-equilibrium molecular dynamics study of subcritical, supercritical and transcritical mixing of liquid-gas systems. Chem Eng Sci 2020;214:115424-35. https://doi.org/10.1016/j.ces.2019.115424.
[41] Mo G, Qiao L. A molecular dynamics investigation of n-alkanes vaporizing into nitrogen: transition from subcritical to supercritical. Combustion and Flame 2017;176:60-71. http://dx.doi.org/10.1016/j.combustflame.2016.09.028.
[42] Yanzhi Zhang MJ, Ping Yi,Yachao Chang,Zhixia He,Qian Wang. A molecular dynamics study of binary-component n-alkane fuel vaporization characteristics at sub/supercritical nitrogen environments. Proceedings of the Combustion Institute 2021;38(2):3303-12. https://doi.org/10.1016/j.proci.2020.06.108.
[43] Wei M, Yang S, Sun H, Wang Y, Guo G. Molecular dynamics simulation of sub/supercritical evaporation with n-butanol/n-heptane blended fuel. Fuel 2021;294. https://doi.org/10.1016/j.fuel.2021.120556.
[44] Chen C, Jiang X. Transport property prediction and inhomogeneity analysis of supercritical n-Dodecane by molecular dynamics simulation. Fuel 2019;244:48-60. https://doi.org/10.1016/j.fuel.2019.01.181.
[45] Wang Y, Gong S, Li L, Liu G. Sub-to-supercritical properties and inhomogeneity of JP-10 using molecular dynamics simulation. Fuel 2020. https://doi.org/10.1016/j.fuel.2020.119696.
[46] Daniel T. Banuti MR, Peter C. Ma, and Matthias Ihme. Seven questions about supercritical fluids towards a new fluid state diagram. American Institute of Aeronautics and Astronautic 2017:10. doi:10.2514/6.2017-1106 .
[47] Woodcock LV. On the Empirical Determination of a Gas–Liquid Supercritical Mesophase and its Phenomenological Definition. Int J Thermophys 2020;41(6). https://doi.org/10.1007/s10765-020-02644-5.

[48] Schienbein P, Marx D. Assessing the properties of supercritical water in terms of structural dynamics and electronic polarization effects. Phys Chem Chem Phys 2020;22(19):10462-79. DOI: 10.1039/c9cp05610f.

[49] Yoon TJ. Thermodynamics, dynamics, and structure of supercritical water at extreme conditions. Physical Chemistry Chemical Physics 2020. DOI: 10.1039/D0CP02288H.

[50] Szymkowicz PG, Benajes J. Single-cylinder engine evaluation of a multi-component diesel surrogate fuel at a part-load operating condition with conventional combustion. Fuel 2018;226:286-97. https://doi.org/10.1016/j.fuel.2018.03.157.

[51] Aleksey Vishnyakov TW, Ashvin Hosangadi, Yee C. Chiew. Molecular models for phase equilibria of alkanes with air components and combustion products I. Alkane mixtures with nitrogen, CO2 and water. Fluid Phase Equilibr 2019. https://doi.org/10.1016/j.fluid.2020.112553.

[52] Xin N, Wang C, Zhang Y, Liu X, He M. Determination of critical properties for binary and ternary mixtures containing dimethyl carbonate and alkanes. The Journal of Supercritical Fluids 2018;137:40-9. https://doi.org/10.1016/j.supflu.2018.02.006.

[53] Chakraborty S, Qiao L. Molecular investigation of sub-to-supercritical transition of hydrocarbon mixtures: Multi-component effect. Int J Heat Mass Tran 2019;145:118629-42. https://doi.org/10.1016/j.ijheatmasstransfer.2019.118629.

[54] Vishnyakov A, Weathers T, Hosangadi A, Chiew YC. Molecular models for phase equilibria of alkanes with air components and combustion products II. Alkane – Oxygen mixtures. Fluid Phase Equilibr 2020. https://doi.org/10.1016/j.fluid.2020.112553.

[55] Manin J, Crua C, Pickett LM. Transcritical mixing of sprays for multi-component fuel mixtures. *Proceedings ILASS–Europe 2017. 28th Conference on Liquid Atomization and Spray Systems.* 2017.

[56] Mao Y, Xia J, Ruan C, Wu Z, Feng Y, Zhu J, et al. An experimental and kinetic modeling study of a four-component surrogate fuel for RP-3 kerosene. Proceedings of the Combustion Institute 2020.

[57] Cao BY, Xie JF, Sazhin SS. Molecular dynamics study on evaporation and condensation of n-dodecane at liquid-vapor phase equilibria. J Chem Phys 2011;134(16):164309. https://doi.org/10.1063/1.3579457.

[58] Collin D. Wick MGM, and J. Ilja Siepmann. Transferable Potentials for Phase Equilibria. 4. United-Atom Description of Linear and Branched Alkenes and Alkylbenzenes. J Phys Chem B 2000;104:8008-16.

[59] Andersen HC. Rattle: A “velocity” version of the shake algorithm for molecular dynamics calculations. Journal of Computational Physics 1983;52:24–34.

[60] Ra Y, Reitz RD. A vaporization model for discrete multi-component fuel sprays. Int J Multiphas Flow 2009;35(2):101-17. doi:10.1016/j.ijmultiphaseflow.2008.10.006.

[61] Ryan T. Butts DF, Roger Krieger, Michael Andrie and Youngchul Ra. Investigation of the Effects of Cetane Number, Volatility, and Total Aromatic Content on HighlyDilute Low Temperature Diesel Combustion. SAE International Journal of Engines 2010.

[62] Li CC. Critical Temperature Estimation for Simple Mixture. The Canadian Journal of Chemical Engineering 1971;49:709–10.

[63] Aleksander Kreglewski WBK. The Critical Constants of Conformal Mixtures. The Journal of Physical Chemistry 1969;73(10):3359– 66.

[64] Martyna METGJ. Understanding Modern Molecular Dynamics: Techniques and Applications. J Phys Chem B 2000;104(2):159-78.

[65] Dahms RN, Oefelein JC. Liquid jet breakup regimes at supercritical pressures. Combustion and Flame 2015;162(10):3648-57. http://dx.doi.org/10.1016/j.combustflame.2015.07.004.

[66] YouXiang Zuo EHS. A Linear Gradient Theory Model for Calculating Interfacial Tensions of Mixtures. J Colloid Interf Sci 1996;182:126–32.

[67] Robert A. Heidemann AMK. The Calculation of Critical Points. AlChE Journal 1980;26(5):769-79.

[68] Manin J PL, Crua C. Microscopic observation of miscible mixing in sprays at elevated temperatures and pressures. *ILASS Americas 27th Annual Conference on Liquid Atomization and Spray Systems.* Raleigh, NC; 2015.

[69] Falgout Z, Rahm M, Sedarsky D, Linne M. Gas/fuel jet interfaces under high pressures and temperatures. Fuel 2016;168:14-21. http://dx.doi.org/10.1016/j.fuel.2015.11.061.

[70] Stephan S, Hasse H. Enrichment at vapour–liquid interfaces of mixtures: establishing a link between nanoscopic and macroscopic properties. International Reviews in Physical Chemistry 2020;39(3):319-49. https://doi.org/10.1080/0144235X.2020.1777705.

[71] Turner CH, Gubbins KE. Effects of supercritical clustering and selective confinement on reaction equilibrium: A molecular simulation study of the esterification reaction. The Journal of Chemical Physics 2003;119(12):6057-67. http://dx.doi.org/10.1063/1.1602691.

[72] Yoshii N, Okazaki S. A large-scale and long-time molecular dynamics study of supercritical Lennard-Jones fluid. An analysis of high temperature clusters. The Journal of Chemical Physics 1997;107(6):2020-33.

[73] Thompson SM, Gubbins KE, Walton JPRB, Chantry RAR, Rowlinson JS. A molecular dynamics study of liquid drops. The Journal of Chemical Physics 1984;81(1):530-42.